

## Reviewed Preprint

v1 • July 8, 2026

Not revised

## ✉ For correspondence:

sillitoe@bcm.edu

^ These authors contributed equally to this work.

**Competing interests:** No competing interests declared

**Funding:** See [page 23](#)

**Reviewing editor:** Katie Hsiao, Children's National, United States

© 2026, Rey Hipolito et al. This article is distributed under the terms of the

[Creative Commons Attribution](#)

[License](#), which permits unrestricted use and redistribution provided that the original author and source are credited.

# Human and mouse cerebellar inhibitory circuits in dystonic crisis and their modulation with therapeutic stimulation

Alejandro G Rey Hipolito<sup>1,2,4,5,^</sup>, Michael P Dew<sup>1,2,4,5,^</sup>, Jason S Gill<sup>3,4,5</sup>, Janelle E Allen<sup>3,4,5</sup>, Karissa A Chesky<sup>3,4</sup>, Mariam Hull<sup>3,4</sup>, Roy V Sillitoe<sup>1,2,4,5</sup>✉

<sup>1</sup>Department of Pathology & Immunology, Baylor College of Medicine, Houston, United States • <sup>2</sup>Department of Neuroscience, Baylor College of Medicine, Houston, United States • <sup>3</sup>Section of Pediatric Neurology and Developmental Neuroscience, Department of Pediatrics Baylor College of Medicine, Houston, United States • <sup>4</sup>Cerebellum Science Center, Texas Children's Hospital, Houston, United States • <sup>5</sup>Jan and Dan Duncan Neurological Research Institute at Texas Children's Hospital, Houston, United States

## eLife Assessment

This **important** study identifies inhibitory cerebellar nuclei neurons as drivers of dystonic crisis and shows that their modulation can both induce and alleviate severe motor symptoms, proposing a cerebello-thalamic circuit mechanism with clear therapeutic relevance. The evidence is **convincing**, supported by rigorous bidirectional optogenetic manipulations, iCNN-to-CL thalamic monosynaptic tracing, and deep brain stimulation experiments, although the specificity of the genetic strategy remains to be fully resolved. The study will be of broad interest to neuroscientists and clinicians working on movement disorders and circuit-based therapies.

<https://doi.org/10.7554/eLife.111315.1.sa3>

## Abstract

Dystonia is a neurological movement disorder characterized by abnormal muscle contractions that, at their most severe, lead to a life-threatening condition - dystonic crisis. Yet, therapeutic options remain limited by our incomplete understanding of what neural circuits underly the condition. Although cerebellar nuclei neurons are implicated in the origin of baseline dystonic symptoms, it is unclear whether their activity drives dystonic crisis. To explore this role, we found that cerebellar abnormalities and neural inhibition were recurring targets in patients with dystonic crisis, implicating cerebellar inhibitory neurons in its development. We devised a mouse genetics approach to test whether inhibitory cerebellar nuclei neurons (iCNNs) induce dystonic crisis. Directional optogenetic modulation of iCNNs induced dystonic crises on-demand and alleviated spontaneous crises in mice that mimic spontaneous dystonic crises. To investigate whether iCNNs interact with other motor areas during dystonic crisis, we identified monosynaptic iCNN projections to the centrolateral nucleus of the thalamus (CL). Deep brain stimulation of the CL alleviated dystonic crises induced by iCNN photoactivation. Our data uncover a cell type-specific cerebellar origin of dystonic crisis and highlight its therapeutic potential.

## Introduction

Dystonia is a neurological movement disorder characterized by sustained or intermittent muscle contractions that cause abnormal movements, postures, or both (1). In the most severe form of the condition, referred to as dystonic crisis (also termed dystonic storm or status dystonicus), the severity and persistence of dystonia require immediate hospitalization (2). Unfortunately,

reaching this stage of devastating symptom intensity leads to mortality in up to 10-12.5% of patients, mostly comprising children with an existing diagnosis of dystonia (3, 4). Relapses are common with a recurrence risk of 25% in the first year, and up to 38.6% at 27 months (5). Treatment options remain limited with variable success and include many complex pharmaceutical strategies or last-resort surgical interventions such as deep brain stimulation (DBS) or an intrathecal or intraventricular baclofen pump (6). Thus, there is an unmet need to develop additional therapeutic options for patients with dystonic crisis, which may be facilitated by identifying the exact neural circuits that drive the condition and targeting them with more precise and effective therapies.

It is unclear what specific neural circuits instigate dystonic crisis and how their dysfunction drives this debilitating condition. However, several lines of evidence suggest that inhibitory neurons and motor structures, especially the cerebellum, contribute to dystonic crisis. Ablation and DBS of motor structures including the globus pallidus and thalamus are therapeutically effective in a subset of patients in dystonic crisis (7), supporting a role for areas within the motor network in this condition. In dystonic crisis, treatments routinely involve drugs that target neural inhibition including benzodiazepines, alpha-2 adrenergic agonists, and anticholinergics (3, 5, 6, 8), suggesting that inhibition in the central nervous system may play a role in the condition just as has been found in other forms of dystonia (9–11). Clinical studies have reported a high incidence of dystonic crisis in patients with cerebral palsy (3, 4, 12, 13), a disorder in which cerebellar dysfunction is thought to play a prominent role (14–16), providing an indirect link to cerebellar dysfunction and dystonic crisis. However, these compelling connections require further investigation.

Although few studies on dystonic crisis exist, preclinical evidence in dystonia highlight a role for cerebellar nuclei neurons, which form the predominant output from the cerebellum to the rest of the motor network (17). In mice, lesioning the superior cerebellar peduncle, the cerebellar outflow tract through which cerebellar nuclei neurons project, was recently shown to cause severe dystonia similar to dystonic crisis (18), suggesting that cerebellar nuclei neurons may contribute to dystonic crisis. In animal studies of paroxysmal dystonia, dystonic episodes correlated with changes in cerebellar nuclei neuron activity. In one study, increased activity of inhibitory cerebellar nuclei neurons (iCNNs) correlated with the onset of dystonic episodes (19), suggesting that the cell type-specificity of cerebellar nuclei neurons may determine their contribution to dystonia. Little is known about the iCNN output pathway, though recent studies have described its termination throughout the brain (20, 21), which may subserve unknown functions in health and disease. Accurately distinguishing the specific roles of the intermingled cerebellar nuclei neurons may be critical for developing better treatments for dystonia and other movement disorders, as was demonstrated for the basal ganglia in a mouse model of Parkinson's disease (22).

To assess the role of iCNNs in dystonic crisis, we started by examining clinical data to study the possible contribution of the cerebellum and inhibitory neurons to dystonic crisis. To complement this clinical study, we sought to manipulate iCNNs in a mouse model of dystonia, and then test whether motor behaviors that resemble dystonic crisis arise. We therefore devised a conditional mouse genetic model to test the hypothesis that modulation of the iCNN output pathway induces dystonic crisis. Using a previously described animal model of dystonia, we genetically expressed opsins in *Ptf1a*-expressing neurons, including iCNNs, and optogenetically modulated them through their projections in the superior cerebellar peduncle. To examine if and how dystonic crises emerge, we combined this approach with behavioral assays and anatomical examination. We also tested whether iCNNs interact with another motor area implicated in dystonia, the centrolateral nucleus of the thalamus (CL), by using anatomical tracing. We then tested the hypothesis that DBS targeted to the CL would modulate the induced dystonic crises. Our data uncover a cerebellar origin of dystonic crisis and inspire the development of targeted therapies.

## Results

### Cerebellar abnormalities and inhibitory neural function are implicated in the incidence and treatment of dystonic crisis in human pediatric-onset dystonia

As previous clinical data only indirectly linked cerebellar function to dystonic crisis (13, 15), we sought to identify more direct clinical evidence that cerebellar dysfunction leads to dystonic crisis and support further preclinical investigations into the precise cerebellar circuits that may be involved. Accordingly, we investigated the clinical characteristics (Table 1) of patients admitted with dystonic crisis (Supplementary Movie 1) at Texas Children's Hospital in Houston, Texas between 2015 and 2019. Of the 49 patients admitted, 19 patients were defined as having dystonia associated with a genetic or progressive etiology while the remaining 30 patients (20 males, 10 females; between 3 months and 20 years of age at admission) had an underlying etiology associated with acquired injury (Figure 1A and Table 1). Of the 30 patients with acquired injury, cerebellar abnormalities were observed in the MRI imaging of 18 (60%; 11 males, 7 females; between 3 months and 18 years of age at admission) patients while 12 of 30 patients (40%; 9 males, 3 females; between 3 and 20 years of age at admission) showed imaging with abnormalities exclusively in the supratentorial regions comprising the cerebral hemispheres, basal ganglia, thalamus, and other structures outside the cerebellum (Figure 1B and Table 1), suggesting that cerebellar abnormalities predispose a substantial number of patients to dystonic crisis. The range of cerebellar abnormalities found in patients with dystonic crisis encompassed focal cerebellar only to focal cerebellar with associated supratentorial to diffuse cerebellar injury (Figure 1C). When comparing the therapies that had clear clinical benefit (as determined by parents and clinicians) across the 30 patients with acquired injury, benzodiazepines and alpha-2 adrenergic agonists were the most widely used and successful (Figure 1D). Patients with cerebellar abnormalities responded preferentially to alpha-2 adrenergic agonists rather than benzodiazepines. Interestingly, benzodiazepines and alpha-2 adrenergic agonists have inhibitory effects on the central nervous system (6, 23, 24). In cerebellar nuclei neurons, the corresponding receptors for these two drugs have been identified (25, 26), and alpha-2 adrenergic agonists have been found to modulate their GABA responses (27), indicating a role for GABAergic cerebellar nuclei neurons in the incidence and treatment of dystonic crisis. Patients with cerebellar abnormalities tended to have longer lengths of hospitalization and days to improvement following their admission with dystonic crisis (Figure 1E). To our knowledge, this is the first clinical evidence directly linking cerebellar developmental abnormalities to dystonic crisis. Together, these results strongly support a role for the cerebellum and inhibitory neural circuitry in driving dystonic crisis in human pediatric-onset dystonia. As iCNNs represent the intersection of cerebellar function, neural inhibition, and cerebellar control of the motor network, we hypothesized that iCNNs instigate the mechanisms that trigger dystonic crisis.

### Photoactivation of the iCNN pathway induces dystonic crises reminiscent of the human condition in a mouse model of dystonia, but not in healthy mice

Although cerebellar nuclei neurons (19, 28) have been implicated in driving the baseline symptoms of dystonia, it remains unclear whether cerebellar nuclei neurons contribute to dystonic crisis. As previous findings and our clinical results support a role for inhibitory cerebellar neurons, we hypothesized that iCNNs specifically instigate dystonic crisis. As previous studies showed increased activity of iCNNs in an animal model of dystonia during paroxysmal episodes of dystonic symptoms, we reasoned that optogenetic activation of iCNNs could induce the more severe dystonic crisis in an animal model of dystonia. To test this, we devised a mouse genetic model that could simultaneously also be manipulated with optogenetics. Since the development of dystonic crises almost exclusively occur in patients with a pre-existing diagnosis of dystonia (5, 29), we sought to optogenetically manipulate the iCNN pathway in a mouse model with robust dystonic

Sex	Age of dystonia onset	Dystonia phenomenology	Etiology	Supratentorial Imaging Findings	Posterior Fossa Imaging Findings	Age of admission for status dystonicus	Description of phenomenology	BZ	α-2	AS	ChemD	VMAT2	None	Dopa	ITB	NmB	Days for improvement
F	10	generalized	Anoxic Brain Injury	Bilateral Cerebral encephalomalacia, thalamic gliosis, basal ganglia signal abnormalities		20	Intermittent stiffening and tremor	x									
M	0.25	generalized	HIE	Basal ganglia signal abnormality, mild cerebral volume loss		17	Dystonia involving proximal portions of all extremities	x		x							2
M	5	generalized	Kernicterus	Mild signal change in basal ganglia		11	Dystonic and dyskinetic movements of all extremities	x									0
M	15	generalized	Prematurity	Severe bilateral cerebral encephalomalacia, thalamic volume loss		15	Generalized dystonia	x	x								0
# M	10	generalized	Prematurity	abnormal signal in bilateral deep gray matter, periventricular leukomalacia		14	Generalized severe increased tone			x							0
\$ F	0.75	generalized	Perinatal Injury	Bilateral occipitoparietal encephalomalacia and periventricular leukomalacia		4	Intermittent opisthotonic posturing	x		x							1
M	0.83	generalized	HIE	Diffuse cortical and deep gray volume loss, thalamic calcifications		12	Extensor posturing										0
M	1	generalized	HIE	Mild cerebral atrophy with severe atrophy of bilateral basal ganglia and thalami		5	Not characterized	x									0
M	3	generalized	NMDA Encephalitis	Basal ganglia encephalomalacia		3	Posturing of all extremities					x				x	1
M	0.17	generalized	HIE	Cerebral volume loss and abnormal signal of bilateral basal ganglia and thalami		10	Mixed spastic/dystonic posturing	x									2
M	1	generalized	Kernicterus	Cerebral volume loss		10	Generalized dystonia					x					2
F	14	generalized	Anoxic Brain Injury	Diffuse cerebral, basal ganglia, and thalamic edema		15	UE/LE without spontaneous movements	x		x							0
M	4	generalized	Anoxic Brain Injury	Cerebral white matter and thalamic volume loss	Mild cerebellar volume loss and focal gliosis in the right cerebellar hemisphere	10	Intermittent generalized episodes of clonus and dystonic tremor	x									0
M	0.52	generalized	Prematurity	Abnormal basal ganglia signal	Deep cerebellar/cerebellar nuclear signal abnormality	2	Generalized dystonia			x							0
F	0.1	generalized	HIE	Encephalomalacia of bilateral cerebral hemispheres, basal ganglia, and thalami	Diffuse cerebellar volume loss	0.25	all extremities with opisthotonic postures						x				7
F	1	generalized	HIE	Encephalomalacia of cerebral hemispheres, basal ganglia, and thalami	Cerebellar atrophy and gliosis	2,375	Opisthotonic posturing with left version	x		x							0
F	5	focal	NMDA Encephalitis	Mild cerebral volume loss	Mild cerebellar volume loss	5	Provokable episodic dystonia						x				7
M	0.58	generalized	Kernicterus	Basal ganglia and hippocampal volume loss and focal left thalamic encephalomalacia	Cerebellar volume loss		Not characterized									x	1
F	14	focal segmental	Anoxic Brain Injury	Cerebral volume loss and abnormal signal in basal ganglia and thalami	Cerebellar atrophy	14	Rigid dystonic posturing					x					
M	1	generalized	HIE	Cerebral encephalomalacia and abnormal basal ganglia and thalamic signal	Cerebellar atrophy and signal change	1.25	Opisthotonic posturing				x						1
% M	1	generalized	Prematurity	Basal ganglia and thalamic volume loss	greater than right, abnormal signal in the dentate nuclei	18	Dystonic lower extremity movements			x							5
& F	1	generalized	Prematurity	Cerebral volume loss	Bilateral Cerebellar hemisphere encephalomalacia and severe atrophy, Pontine atrophy	18	trunk present in episodes with spasticity										9
£ M	0.5	generalized	Perinatal Injury	Focal occipital and parietal encephalomalacia	Bilateral cerebellar encephalomalacia	7	Intermittent episodes with preserved range of motion	x									0
M	1.75	generalized	In Utero (SOD)	Corpus callosal hypoplasia	Cerebellar atrophy	1.75	Increased axial and upper extremity tone							x			3
M	13	focal segmental	Traumatic Brain Injury	Basal ganglia encephalomalacia	Cerebellar signal abnormalities	13	Generalized dystonia of upper greater than lower extremities									x	1
M	16	generalized	Infectious (West Nile virus)	Diffuse signal abnormalities of basal ganglia, thalamus, and cortex	Atrophy of the left greater than right cerebellar hemisphere	18	Upper extremities held in flexion										1
M	10	generalized	HIE	Cerebral, basal ganglia, and thalamic signal abnormalities	Cerebellar atrophy and signal change	16	Rigid upper extremity flexion lower extremity extension	x		x							3
c.F	1.92	focal segmental	NMDA Encephalitis	Normal imaging	Left focal cerebellar encephalomalacia	1.92	Opisthotonic posture with right version				x						0
F	3	generalized	Prematurity	Cerebral volume loss	Atrophic cerebellum with hypoplastic pons	10	Opisthotonic extension with right version	x		x							3
M	1	generalized	HIE	Bilateral cerebral and deep gray encephalomalacia	Cerebellar volume loss and gliosis with prominent cerebellar folia	1.17	Variable dystonic movements observed	x		x							1

Abbreviations of treatments with clinical benefit: BZ = benzodiazepine; α-2 = Alpha-2 agonists; AS = antispasmodic agents; ChemD = chemodenervation; VMAT2 = VMAT-2 inhibitor; None = no therapy with clinical benefit; Dopa = dopaminergic agonism; ITB = intrathecal baclofen pump; NmB = neuromuscular blockade.

**Table 1. Clinical characteristics of patients with dystonic crisis, also known as status dystonicus (SD).**

Table outlines clinical characteristics of 30 patients admitted to Texas Children’s Hospital from 2015-2019 with acquired etiologies of dystonic crisis. Top grouping includes patient with only supratentorial findings, while bottom grouping includes those with cerebellar findings. Summarized imaging findings are as indicated in the respective columns. Ages are shown in years. “Dystonia phenomenology” refers to the description of dystonia based on consensus classifications while “Description of phenomenology” indicates the patient specific presentation of dystonia during SD. Patients with imaging depicted in figure 1 are as follows: # = top left, \$ = bottom left, € = top middle, % = bottom middle, £ = top right, & = bottom right. Abbreviations of treatments with clinical benefit: BZ = benzodiazepine; α-2 = Alpha-2 agonists; AS = antispasmodic agents; ChemD = chemodenervation; VMAT2 = VMAT-2 inhibitor; None = no therapy with clinical benefit; Dopa = dopaminergic agonism; ITB = intrathecal baclofen pump; NmB = neuromuscular blockade.

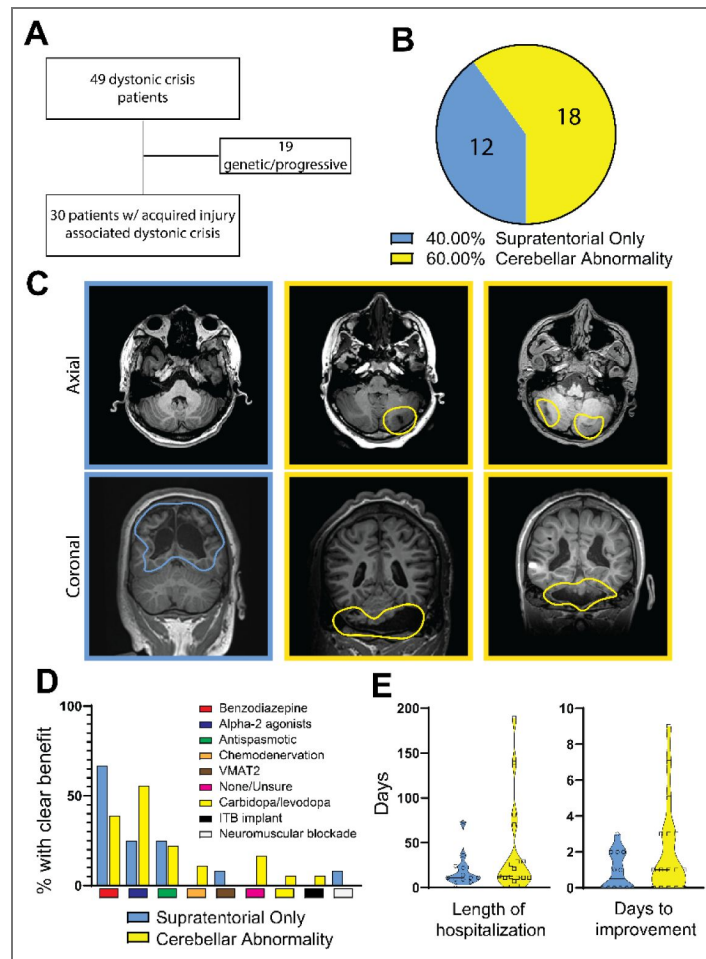


**Figure 1. Cerebellar abnormalities and inhibitory neural function are implicated in the incidence and treatment of dystonic crisis.**

(A) Patient flow chart showing the division of 49 patients with dystonic crisis into groups based on the etiology of their dystonia: genetic/progressive (19 patients) or acquired injury (30 patients). (B) Percentage of patients admitted for dystonic crisis that had abnormalities in the cerebellum with or without supratentorial findings or only supratentorial abnormalities (blue) on imaging. (C) Examples of imaging in patients with supratentorial only injury (left column, outlined in blue) or cerebellar findings (middle and right column, outlined in yellow with abnormalities encircled). The top row depicts the axial plane through the cerebellum on T1 weighted imaging. The top left depicts the cerebellum at the level of the superior cerebellar peduncles, the top middle depicts a sequela of isolated left cerebellar hemispheric stroke, the top right depicts bilateral cerebellar hemispheric encephalomalacia (outlined in blue). The bottom row depicts the coronal plane through the cerebellum and the parietal lobe on T1 weighted imaging. The bottom right shows the normal cerebellum with extensive bilateral periventricular encephalomalacia. The bottom middle and right show patients with extensive bilateral cerebellar encephalomalacia. (D) Comparison of therapies that had clear clinical benefit across the 30 patients with acquired injury associated with dystonic crisis. Benzodiazepines and alpha-2 adrenergic agonists were the most widely used and successful. Patients with cerebellar abnormalities responded preferentially to alpha-2 adrenergic agonists rather than benzodiazepines. (E) Patients with cerebellar abnormalities tended to have longer lengths of hospitalization (Unpaired t-test with Welch’s correction  $p=0.167$ ,  $f=0.001$ ) and days to improvement (Unpaired t-test with Welch’s correction  $p=0.104$ ,  $f=0.004$ ) following their admission with dystonic crisis.

symptoms. The *Ptf1a<sup>Cre</sup>;Vglut2<sup>fx/fx</sup>* mouse (30, 31) was chosen because of the cerebellar specificity of the manipulation that gives rise to dystonia, its *Ptf1a*-specific expression of Cre, and the severity of its dystonic symptoms (Figure 2A). As *Ptf1a* is expressed in iCNNs among other areas (32, 33), it allowed cre-inducible expression within iCNNs to manipulate their activity and visualize their anatomy with genetic precision. In these mutant mice, vesicular glutamate transporter 2 (VGLUT2) is genetically excised in *Ptf1a*-expressing neurons. As only inferior olive neurons, a major cerebellar input to cerebellar Purkinje cells, express *Ptf1a* and *Vglut2* (32), this manipulation selectively silences neurotransmission from olivary climbing fibers to the cerebellum (Figure 2A), resulting in a robust dystonic phenotype described previously (30). These mutant mice exhibit dystonic symptoms of mild-to-moderate twisting postures in the limbs, trunk, head, and/or tail interrupted by random and intermittent periods of severe generalized dystonia in several body parts reminiscent of human dystonic crises, making them a great model in which to investigate whether iCNN activity triggers dystonic crisis. Similar to human patients in which the same underlying genetic mutation may result in a spectrum of dystonic symptoms across patients (34, 35), the severity of the underlying dystonic symptoms in the *Ptf1a<sup>Cre</sup>;Vglut2<sup>fx/fx</sup>* mouse can vary between animals. To selectively manipulate the iCNN pathway in these mice using optogenetics, we crossed the *Ptf1a<sup>Cre</sup>;Vglut2<sup>fx/fx</sup>* mice with *ROSA<sup>lsl-Chr2/EYFP</sup>* mice to generate *Ptf1a<sup>Cre</sup>;Vglut2<sup>fx/fx</sup>;ROSA<sup>lsl-Chr2/EYFP</sup>* mice (Figure 2B). To confirm that iCNNs selectively expressed the Chr2 construct in the *Ptf1a<sup>Cre</sup>;Vglut2<sup>fx/fx</sup>;ROSA<sup>lsl-Chr2/EYFP</sup>* mice, we performed *in situ* hybridization assays for the YFP tag in the construct, *Vgat* (inhibitory marker), and *Vglut2* (excitatory marker). Robust co-labeling of YFP and *Vgat*, but not *Vglut2*, was observed in the mutant deletion mice (Figure 2C and Supplemental Figure 1, n=3 animals). To selectively manipulate the iCNN pathway and avoid activation of Purkinje cell terminals (which also express *Ptf1a*) in the cerebellar nuclei, we targeted iCNN axons by bilaterally implanting optical fibers over the superior cerebellar peduncle, the white matter tract through which extracerebellar cerebellar nuclei neuron projections pass (17) (Figure 2D and Supplemental Figure 2). The selective manipulation of cerebellar nuclei neurons by targeting the superior cerebellar peduncle has been similarly employed to create an animal lesion model of dystonic crisis (18) and to therapeutically treat refractory dystonia in patients (36, 37). The behavior of experimental mice in an open field was video recorded and data from two minutes before and during stimulation were analyzed (470 nm light; 50 Hz square pulses;  $\geq 1$  mW at fiber tip). To detect changes in the incidence of dystonic crises, we measured the percentage of time that a mouse spent in a dystonic crisis during each period (before vs during stimulation). Throughout this study, we define a dystonic crisis in mice as observable dystonic limb contractions, limb hyperextensions and/or overt postures in at least two body parts in addition to severely limited ambulation for at least 3 seconds, a sufficient time to confidently determine that ambulation was restricted (rather than due to voluntary resting) and a result of abnormal muscle activity (Supplementary Movie 2).

Photoactivation of the iCNN pathway induced severe dystonic crises on-demand which was clearly observable in videos (Figure 2E and Supplementary Movie 2; i.e. extended limbs, rigidity throughout the body, stiff tail, splayed digits, toppling over, severely impaired ambulation). The photoinduced dystonic crises were similar to the most severe spontaneous periods of dystonia observed in these mutant mice and reminiscent of the acute, severe episodes of dystonia observed in another murine model of dystonic crisis (18). The photoactivation period was marked by a significant increase in the percentage of time spent in a dystonic crisis during stimulation (92%) compared to before stimulation (34%), supporting that a dystonic crisis was induced (Figure 2F, n=9 animals; p=0.0039, Wilcoxon matched-pairs signed rank test, two-tailed). The photoinduced dystonic crisis occurred within 9 seconds of stimulation onset (Supplemental Figure 3A; n=9 animals), persisted throughout the duration of the light stimulation, and did not end until 38 seconds after the stimulation ended (Supplemental Figure 3B; n=9 animals).

Although dystonic crisis occurs in patients with pre-existing dystonia in most cases, it is possible for otherwise healthy patients to develop a dystonic crisis (5, 29). Likewise, it may be possible that the iCNN pathway may broadly generate general dystonic movements rather than specifically trigger dystonic crisis in the context of a pre-existing dystonic condition. To test this, we repeated this optogenetic experiment in otherwise healthy mice with an opsin (*Ptf1a<sup>Cre</sup>;ROSA<sup>lsl-Chr2/EYFP</sup>*).

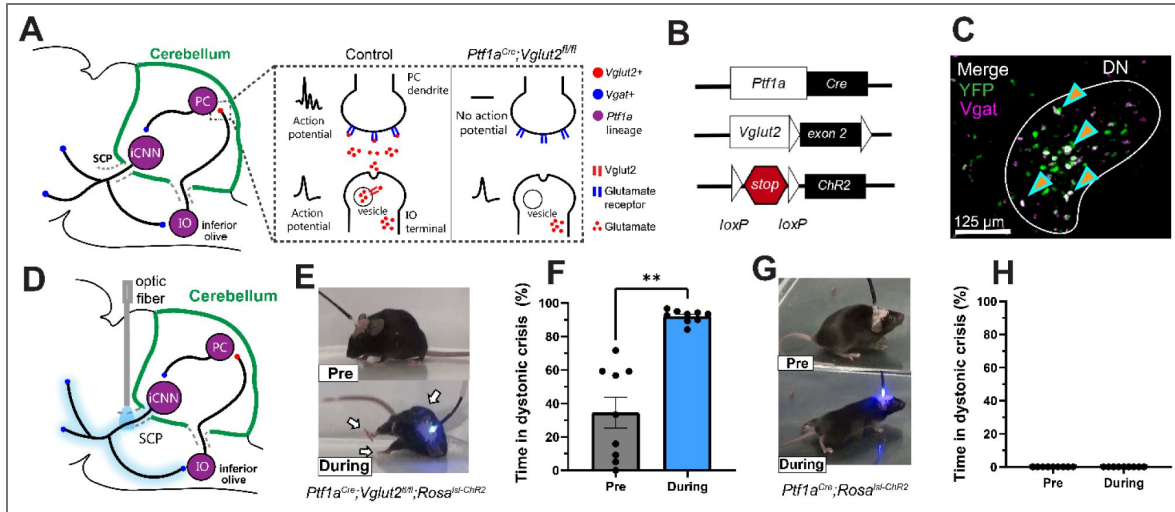


**Figure 2. Photoactivation of the inhibitory cerebellar nuclei neuron (iCNN) pathway induces dystonic crises reminiscent of the human condition in *Ptf1a<sup>Cre</sup>;Vglut2<sup>fx/fx</sup>;ROSA<sup>Isl-Chr2</sup>/EYFP* mice with existing dystonia, but not in otherwise healthy mice.**

(A) Schematic showing the genetic manipulation in *Ptf1a<sup>Cre</sup>;Vglut2<sup>fx/fx</sup>* mice that selectively silenced olivocerebellar synapses, which causes dystonia. (B) Using the *Ptf1a<sup>Cre</sup>* driver, exon 2 of *Vglut2* was selectively removed and *Vglut2* deleted from the inferior olive. Concurrently, the loxP sites surrounding a stop signal preceding Chr2-YFP were removed, allowing expression of Chr2-YFP in *Ptf1a*-expressing neurons including inferior olivary neurons, Purkinje cells, and iCNNs. (C) *In situ* image showing co-labeling of YFP and Vgat in the cerebellar nuclei. (D) Schematic showing the selective photoactivation iCNNs through their projections in the superior cerebellar peduncle. (E) Photoactivation of the iCNN pathway induced a dystonic crisis on-demand. (F) In *Ptf1a<sup>Cre</sup>;Vglut2<sup>fx/fx</sup>;ROSA<sup>Isl-Chr2</sup>/EYFP* mice, photoactivation of the iCNN pathway significantly increased the percentage of time spent in dystonic crisis when comparing before and during stimulation (n=9 animals; p=0.0039, Wilcoxon matched-pairs signed rank test, two-tailed). (G) Photoactivation of the iCNN pathway in healthy *Ptf1a<sup>Cre</sup>;ROSA<sup>Isl-Chr2</sup>/EYFP* mice resulted in abnormal movements, but not dystonic crises. (H) Photoactivation of the iCNN pathway did not influence the percentage of time spent in dystonic crisis when comparing before and during stimulation (n=9 animals). Error bars are defined as standard error of the mean. SCP, superior cerebellar peduncle; PC, Purkinje cell; iCNN, inhibitory cerebellar nuclei neuron; IO, inferior olive; DN, dentate cerebellar nucleus.

Photoactivation of the iCNN pathway in healthy mice ( $Ptf1a^{Cre};ROSA^{Isl-Chr2/EYFP}$ ) did not result in dystonic crises (Figure 2G and Supplementary Movie 3) as the percentage of time in crisis remained 0 before and during the stimulation (Figure 2H;  $n=9$  animals). However, iCNN photoactivation did lead to abnormal movement and short, intermittent, mild dystonic movements. Almost instantaneously with the onset of stimulation, the mouse was observed to be more tense, lowered its body to the ground as if crawling, widened its hind legs, dragged its trunk along the floor while walking, and appeared to “waddle” with slow and clunky locomotion forward and wide steps (Figure 2G and Supplementary Movie 3). These data suggest that the pre-existing dystonic state of  $Ptf1a^{Cre};Vglut2^{fx/fx};ROSA^{Isl-Chr2/EYFP}$  mice sensitizes the iCNN pathway to trigger dystonic crises. As dystonic crisis predominantly arises in patients with a pre-existing diagnosis of dystonia, these results further support a role for the iCNN pathway in the origin of dystonic crises.

## Photoinhibition of the iCNN pathway alleviates spontaneous dystonic crises in a mouse model of dystonia

As photoactivation of the iCNN pathway induced dystonic crisis, we reasoned that photoinhibition of the iCNN pathway would alleviate spontaneous dystonic crises in  $Ptf1a^{Cre};Vglut2^{fx/fx}$  mice. To test this, we generated  $Ptf1a^{Cre};Vglut2^{fx/fx};ROSA^{Isl-Arch}$  mice expressing the inhibitory opsin, archaerhodopsin, and targeted photostimulation to the iCNN pathway as previously described (Figure 3A). As we were interested in detecting a reduction in the time spent in dystonic crisis and the severity of dystonia varies across individual mice, we selected  $Ptf1a^{Cre};Vglut2^{fx/fx};ROSA^{Isl-Arch}$  mice that had severe dystonic crises frequently. To address the presence of possible lags in the onset of therapeutic effects of photoinhibition, as previously observed in treatments of dystonic patients (38–41) and animal models (30), we repeated the experiment over four consecutive days. To establish a baseline for how much time the mice spend in dystonic crisis over a 35-minute session without optogenetic manipulation, we performed the experiment without any photostimulation on Day 0 (Figure 3B). To test whether photostimulation influenced the percentage of time spent in dystonic crisis, video was recorded for five minutes before and five minutes during stimulation (561 nm light; continuous light;  $\geq 1$  mW at fiber tip). To increase confidence that any behavioral change was a result of optogenetic manipulation, we repeated the stimulation paradigm three times on each day, resulting in a 35-minute session for each day (Figure 3B). For each day, we averaged the percentage of time spent in crisis before and during the stimulation periods and then compared the resulting values for statistical significance.

To test whether photoinhibition of the iCNN pathway led to a same-day reduction in dystonic crises, we first performed the experiment without any photostimulation on Day 0 (Figure 3b). As expected on Day 0 when no photostimulation was given, we did not find a significant change in the percentage of time spent in dystonic crisis when comparing periods corresponding to before and during stimulation (93% vs 94%;  $p=0.6875$ ) in severely dystonic  $Ptf1a^{Cre};Vglut2^{fx/fx};ROSA^{Isl-Arch}$  mice (Figure 3D,  $n=7$  animals, Wilcoxon matched-pairs signed rank test, two-tailed). Remarkably, same-day photoinhibition of the iCNN pathway alleviated spontaneous dystonic crises and rescued mobility in these mice (Figure 3C and Supplementary Movie 4) as shown by a significant decrease in the percentage of time spent in dystonic crisis when comparing before versus during photostimulation on Day 1 (90% vs 66%;  $p=0.0156$ ), Day 2 (82% vs 57%;  $p=0.0156$ ), and Day 3 (79% vs 54%;  $p=0.0156$ ) (Figure 3D;  $n=7$  animals, Wilcoxon matched-pairs signed rank test, two-tailed).

As our previous analysis for each day averaged the effects of three stimulations over 35 minutes, we wondered whether the observed therapeutic effects were triggered immediately by the first stimulation or whether they developed progressively over the course of the three stimulations of each day. To test this, the percentage of time in dystonic crisis across five-minute periods on a given day was compared (Figure 3E). On Day 0, when comparing the first five minute period (1–5) to each subsequent five-minute time period (6–10, 11–15, 16–20, 21–25, 26–30, 31–35), there was no significant change (Figure 3E,  $n=7$  animals; for 1-5 vs 6-20,  $p=0.7500$ ; for 1-5 vs 11-15,  $p=0.0625$ ; for 1-5 vs 16-20,  $p=0.9219$ ; for 1-5 vs 21-25,  $p=0.8750$ ; for 1-5 vs 26-30,  $p=0.6719$ ; for 1-5 vs

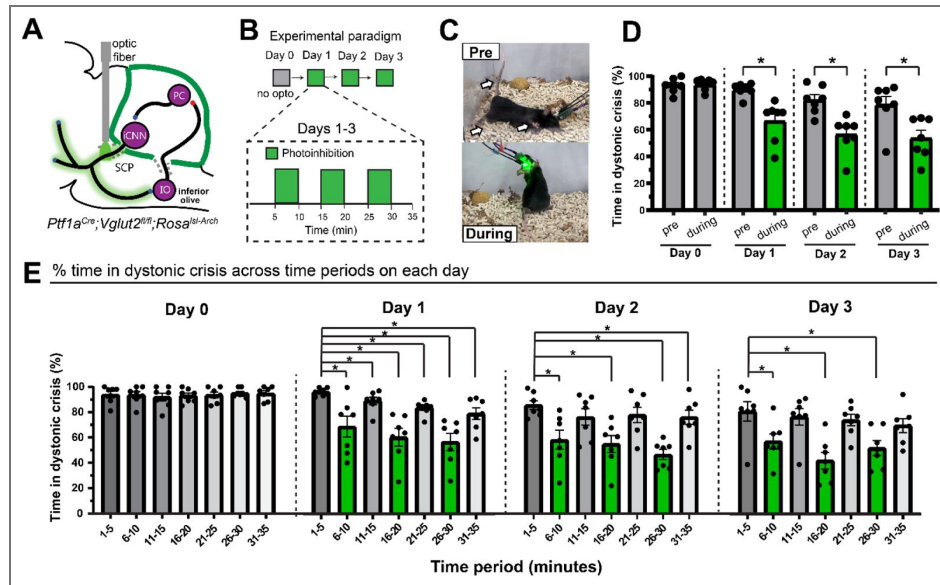


**Figure 3. Photoinhibition of the inhibitory cerebellar nuclei neuron (iCNN) pathway alleviates the spontaneous dystonic crises in *Ptf1a<sup>Cre</sup>;Vglut2<sup>fx/fx</sup>;ROSA<sup>Isl-Arch</sup>/EYFP* mice with existing dystonia.**

(A) Schematic showing the selective photoinhibition of the iCNN pathway by implanting optical fibers into the superior cerebellar peduncle of *Ptf1a<sup>Cre</sup>;Vglut2<sup>fx/fx</sup>;ROSA<sup>Isl-Arch</sup>* mice. (B) Schematic showing the four-day experimental paradigm. (C) Photoinhibition of the iCNN pathway alleviated dystonic crises in *Ptf1a<sup>Cre</sup>;Vglut2<sup>fx/fx</sup>;ROSA<sup>Isl-Arch</sup>* mice as shown in (D) by a significant decrease in the percentage of time spent in crisis when comparing pre versus during photostimulation on Day 1 ( $p=0.0156$ ), Day 2 ( $p=0.0156$ ), and Day 3 ( $p=0.0156$ ) (E) Photoinhibition on Day 1 reduced dystonic crises across all time periods (for 1-5 vs 6-20,  $p=0.0312$ ; for 1-5 vs 11-15,  $p=0.0156$ ; for 1-5 vs 16-20,  $p=0.0156$ ; for 1-5 vs 21-25,  $p=0.0156$ ; for 1-5 vs 26-30,  $p=0.0156$ ; for 1-5 vs 31-35,  $p=0.0156$ ). Photoinhibition on Day 2 alleviated crises across several time periods (for 1-5 vs 6-20,  $p=0.0156$ ; for 1-5 vs 11-15,  $p=0.2345$ ; for 1-5 vs 16-20,  $p=0.0156$ ; for 1-5 vs 21-25,  $p=0.2969$ ; for 1-5 vs 26-30,  $p=0.0156$ ; for 1-5 vs 31-35,  $p=0.0469$ ). Photoinhibition on Day 3 reduced crises across several time periods (for 1-5 vs 6-20,  $p=0.0156$ ; for 1-5 vs 11-15,  $p=0.2188$ ; for 1-5 vs 16-20,  $p=0.0156$ ; for 1-5 vs 21-25,  $p=0.1562$ ; for 1-5 vs 26-30,  $p=0.0156$ ; for 1-5 vs 31-35,  $p=0.0781$ ). For all statistics:  $n=7$  animals, Wilcoxon matched-pairs signed rank test, two-tailed, error bars are defined as standard error of the mean.

31-35,  $p=0.8438$ ; Wilcoxon matched-pairs signed rank test, two tailed). When making the same comparison on Day 1, we found a significant reduction in dystonic crises across all time periods (Figure 3E [↗](#),  $n=7$  animals; for 1-5 vs 6-20,  $p=0.0312$ ; for 1-5 vs 11-15,  $p=0.0156$ ; for 1-5 vs 16-20,  $p=0.0156$ ; for 1-5 vs 21-25,  $p=0.0156$ ; for 1-5 vs 26-30,  $p=0.0156$ ; for 1-5 vs 31-35,  $p=0.0156$ ; Wilcoxon matched-pairs signed rank test, two tailed). On Day 2, we found a significant reduction in dystonic crisis across several time periods (Figure 3E [↗](#),  $n=7$  animals; for 1-5 vs 6-20,  $p=0.0156$ ; for 1-5 vs 11-15,  $p=0.2345$ ; for 1-5 vs 16-20,  $p=0.0156$ ; for 1-5 vs 21-25,  $p=0.2969$ ; for 1-5 vs 26-30,  $p=0.0156$ ; for 1-5 vs 31-35,  $p=0.0469$ ; Wilcoxon matched-pairs signed rank test, two tailed). Day 3 showed a similar significant reduction during stimulation periods (Figure 3E [↗](#),  $n=7$  animals; for 1-5 vs 6-20,  $p=0.0156$ ; for 1-5 vs 11-15,  $p=0.2188$ ; for 1-5 vs 16-20,  $p=0.0156$ ; for 1-5 vs 21-25,  $p=0.1562$ ; for 1-5 vs 26-30,  $p=0.0156$ ; for 1-5 vs 31-35,  $p=0.0781$ ; Wilcoxon matched-pairs signed rank test, two tailed). As the significant reductions in the time spent in dystonic crisis on Day 2 and Day 3 predominantly occur during stimulation periods and not non-stimulation periods, they support the idea that the alleviation of dystonic crises is a consequence of our optogenetic manipulation rather than other confounding variables like exhaustion or familiarity with the environment. These results further suggest that photoinhibition of the iCNN pathway has short-term, same-day, cumulative therapeutic effects on dystonic crisis.

To explore whether any long-term, multiday, cumulative therapeutic effects may have occurred across days, the percentage of time in dystonic crisis was compared across the pre stimulation periods and during stimulation periods across days (Supplemental Figure 4 [↗](#)). For the pre stimulation periods when comparing Day 1 (the first day of stimulation) against Day 2 and Day 3, we report a trend toward a reduction in dystonic crises, but it is not statistically significant (Supplemental Figure 4A [↗](#),  $n=7$  animals; for Day 1 vs Day 2,  $n=0.0625$ ; for Day 1 vs Day 3,  $n=0.0781$ ; Wilcoxon matched-pairs signed rank test, two tailed). For the during stimulation periods, we found a significant reduction in dystonic crises when comparing Day 1 to Day 2 and Day 3 (Supplemental Figure 4B [↗](#),  $n=7$  animals; for Day 1 vs Day 2,  $n=0.0312$ ; for Day 1 vs Day 3,  $n=0.0156$ ; Wilcoxon matched-pairs signed rank test, two tailed). These results suggest that the photoinhibition of the iCNN pathway also has long-term, multiday, cumulative therapeutic effects on dystonic crisis.

Together, these results suggest that photoinhibition of iCNN activity immediately alleviates spontaneous dystonic crises in mice with severe dystonia, and that these beneficial therapeutic effects accumulate over time.

## iCNNs send direct projections to the centrolateral nucleus of the thalamus (CL)

As dystonia is thought to result from aberrant interactions across structures in the motor network ([42](#)), we reasoned that the iCNN pathway interacts with other structures in the motor network to control the onset of a dystonic crisis. Emerging evidence in patients ([34](#), [43–45](#)) and animal models ([30](#), [46](#), [47](#)) support a role for the cerebello-thalamo-basal ganglia pathway in several forms of dystonia, and anatomical studies in non-human primates and animal models have revealed that the cerebellar nuclei interact with the basal ganglia through the CL ([48](#), [49](#)). However, it is thought that these cerebello-thalamic projections predominantly originate from excitatory, not inhibitory, cerebellar nuclei neurons ([20](#), [49](#), [50](#)). Moreover, it remains unknown whether the cerebello-thalamo-basal ganglia pathway contributes to dystonic crisis. To investigate whether iCNNs form a part of the cerebello-thalamo-basal ganglia pathway, we hypothesized that there may be a previously unknown monosynaptic projection from iCNNs to the CL. In *Ptf1a<sup>Cre</sup>;Vglut2<sup>fx/fx</sup>;ROSA<sup>Isl-Chr2/EYFP</sup>* mice, we identified axons labeled with ChR2-EYFP in the CL (Figure 4A [↗](#)), suggesting that there may indeed be monosynaptic iCNN projections. However, as these projections could originate from any *Ptf1a*-expressing region (including the hypothalamus, retina, spinal cord, cerebellum, brainstem, or forebrain), we designed an experiment to determine whether iCNNs have a robust monosynaptic projection to the CL using a combination of intersectional genetics and injected neural tracers. To genetically label only the cell bodies of *Ptf1a*-expressing neurons like iCNNs, we crossed *Ptf1a<sup>Cre</sup>;Vglut2<sup>fx/fx</sup>* with a cre-dependent Sun1 (a small nuclear envelope

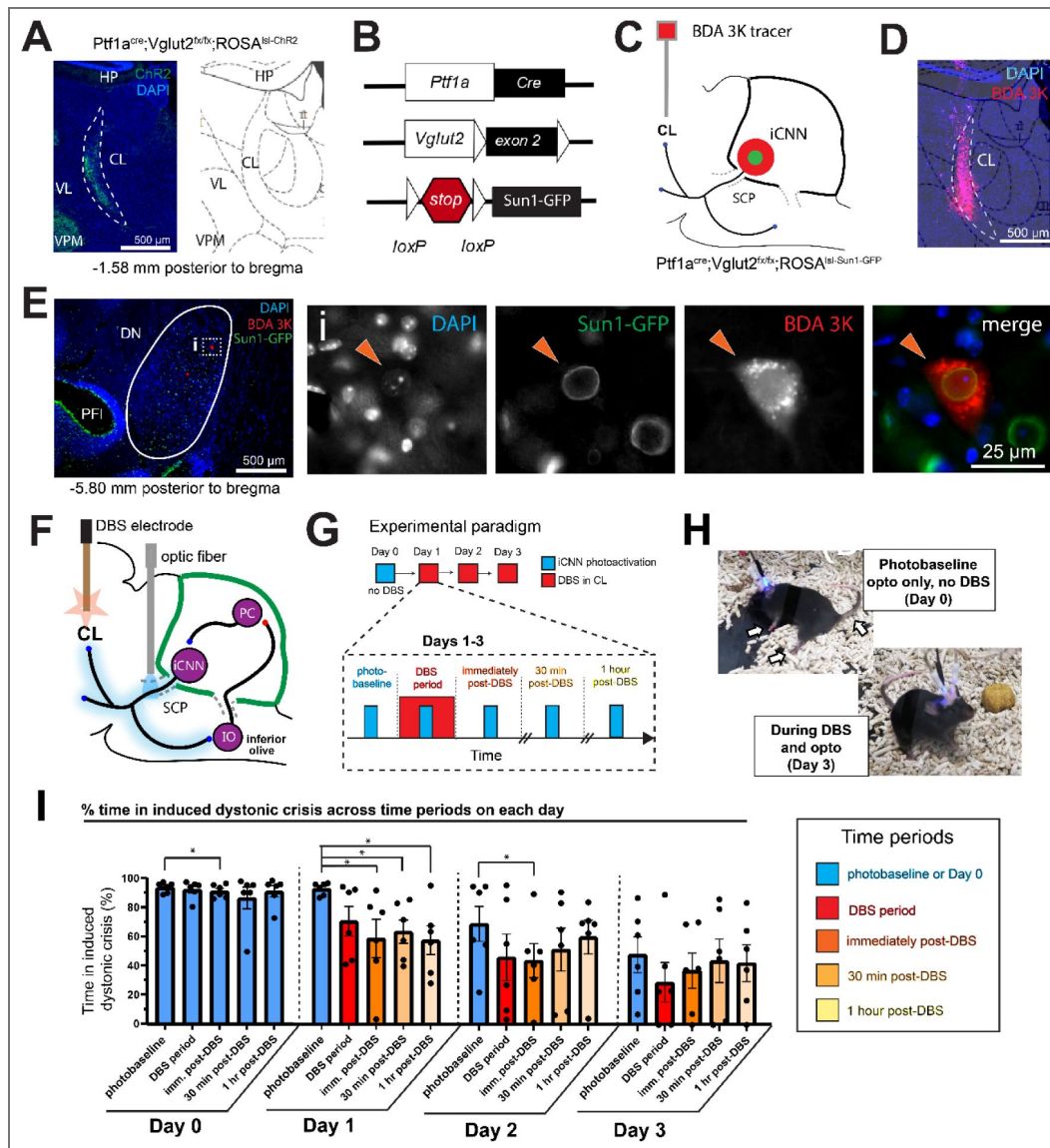
protein) reporter line to generate *Ptf1a<sup>Cre</sup>;Vglut2<sup>fx/fx</sup>;ROSA<sup>lsl-Sun1-GFP</sup>* mice (Figure 4B [↗](#)). To retrogradely label the cell bodies of iCNs that may project to the CL, we bilaterally injected BDA 3K (a predominantly retrograde neural tracer ([51](#), [52](#))) into the CL (Figure 4C-D [↗](#)). We found co-labeling of DAPI, BDA 3K, and Sun1-GFP in the cerebellar nuclei (Figure 4E [↗](#), **inset i; orange ticks**), suggesting that iCNs monosynaptically project to the CL. We found co-labeling of these three markers across all three major cerebellar nuclei comprising the fastigial, interposed, and dentate cerebellar nuclei (Supplemental Figure 5 [↗](#)). These data identify a specific cerebello-thalamic anatomical pathway through which iCNs could control and/or contribute to the onset of dystonic crisis.

## DBS of the CL alleviates dystonic crises induced by iCNN photoactivation

As our data showed that iCNN photoactivation induces dystonic crises and that iCNs project to the CL, we sought to test whether iCNs and the CL interact to control the onset of dystonic crisis and reflect a possible therapeutic node. Specifically, we wondered whether CL activity is required to induce the dystonic crises triggered by the iCNN pathway. This importance of CL activity in dystonia has been highlighted by previous studies showing that the disruption of CL activity with pharmacological agents, electrolytic lesions, or DBS can alleviate dystonic symptoms in animal models of dystonia ([18](#), [30](#), [46](#), [49](#)) including the *Ptf1a<sup>Cre</sup>;Vglut2<sup>fx/fx</sup>* model. Thus, we reasoned that if the iCNN pathway, specifically, induces dystonic crises through the CL, then DBS of the CL will alleviate the dystonic crises induced by iCNN photoactivation.

To test this in the *Ptf1a<sup>Cre</sup>;Vglut2<sup>fx/fx</sup>;ROSA<sup>lsl-Chr2/EYFP</sup>* mice, we unilaterally implanted an optical fiber over the superior cerebellar peduncle and bilaterally implanted bipolar DBS electrodes into the CL (Figure 4F [↗](#) and Supplemental Figure 6 [↗](#)). To account for possible delays in the therapeutic effect of DBS as previously observed in patients and animal models, we repeated the experiment over four consecutive days. Each day consisted of an 86-minute session divided into five distinct periods: photobaseline, DBS period, immediately post-DBS, 30 minutes post-DBS, and 1 hour post-DBS (Figure 4G [↗](#)). During each distinct period, a 2-minute stimulation of blue light (470 nm light; 50 Hz square pulses;  $\geq 1$  mW at fiber tip) was administered followed by 2 minutes of no light stimulation. This paradigm was repeated three times for each distinct period. The percentage of time spent in a dystonic crisis was quantified for each of the three light pulses, and the average of these values was analyzed. To establish a baseline for how much time the mice spend in dystonic crises induced by iCNN photoactivation, we performed this experiment without any DBS on Day 0 (Figure 4G [↗](#)). We administered DBS on Days 1-3. We only performed DBS in the DBS period for 10 minutes (130 Hz, 60  $\mu$ s, 30  $\mu$ A), starting with the onset of the first light pulse and ending with the offset of the third light pulse.

First, we analyzed whether CL-DBS led to same-day changes in the time in induced dystonic crisis across the five time periods (Figure 4I [↗](#)). On Day 0, the percentage of time in induced crisis across the five time periods remained mostly the same (between 83-94%), though there was a statistically significant reduction during photobaseline compared to the immediately post-DBS period (94% vs 91%;  $p=0.0312$ ) (Figure 4I [↗](#);  $n=6$  mice, Wilcoxon matched-pairs signed rank test, two tails). This suggested that iCNN photoactivation reliably and consistently induced dystonic crises throughout the 86-minute session. On Day 1, when comparing between the photobaseline and all subsequent time periods after DBS was administered, we found a marked reduction in the time spent in induced crisis when comparing the same-day photobaseline to during DBS (93% vs 70%;  $p=0.0625$ ), immediately post-DBS (93% vs 58%;  $p=0.0312$ ), 30 minutes post-DBS (93% vs 63%;  $p=0.0312$ ), and 1 hour post-DBS (93% vs 57%;  $p=0.0312$ ) (Supplementary Movie 5 [↗](#) and Figure 4I [↗](#),  $n=6$  animals, Wilcoxon matched-pairs signed rank test, two tails). This progression suggests a short-term, delayed therapeutic effect of CL-DBS on iCNN-mediated dystonic crises. On Day 2, while the same general trend in reduced time in induced dystonic crisis following CL-DBS was observed, there was only a statistically significant reduction from the same-day baseline to immediately post-DBS (69% vs 44%;  $p=0.0312$ ) (Figure 4I [↗](#),  $n=6$  animals, Wilcoxon matched-pairs signed rank test, two tails). On Day 3, we did not find statistically significant changes though the same general trend in



reduced crisis time following DBS can be seen (Figure 4I). Importantly, a trending decrease in dystonic crises across days can be appreciated (Figure 4H-I), especially in the photobaseline periods, which may explain the lack of statistically significant comparisons on Days 2-3. These data suggest that CL-DBS causes long-term, multi-day, therapeutic changes that alleviate dystonic crises induced by iCNN photoactivation.

To further explore whether CL-DBS led to long-term, multi-day therapeutic changes in the induced dystonic crisis time, we compared the time in induced dystonic crisis for each period across Days 0-3 (Supplemental Figure 7). When comparing the photobaseline period across days (Supplemental Figure 7A), we observed a clear reduction in the time in induced crisis on Day 2 (69%) and Day 3 (48%) compared to Day 0 (94%) and Day 1 (93%). This corresponded to the days after CL-DBS had been administered at least once, suggesting that CL-DBS likely led to this long-term therapeutic change in dystonic crisis induction. However, we only detected a statistically significant reduction when comparing Day 0 with Day 3 (Supplemental Figure 7A,  $n=6$  animals,  $p=0.0312$ , Wilcoxon matched pairs signed rank test, two tails). For the DBS period, when comparing against the time in crisis on Day 0 (92%), we observed a trending but non-significant reduction on Day 1 (92% vs 70%;  $p=0.1562$ ) and a statistically significant reduction on Day 2 (92% vs 46%;  $p=0.0312$ ) and Day 3 (92% vs 29%;  $p=0.0312$ ) (Supplementary Movie 5 and Supplemental Figure 7A,  $n=6$  animals, Wilcoxon matched-pairs signed rank test, two tails). For immediately post-DBS, the induced attack time on Day 0 significantly decreased on Day 1 (91% vs 58%;  $p=0.0312$ ), Day 2 (91% vs 44%;  $p=0.0312$ ), and Day 3 (91% vs 37%;  $p=0.0312$ ) (Supplemental Figure 7A,  $n=6$  animals, Wilcoxon matched-pairs signed rank test, two tails). For 30 minutes post-DBS, the induced crisis time on Day 0 decreased on Day 1 (86% vs 63%;  $p=0.0312$ ), Day 2 (86% vs 51%;  $p=0.01562$ ), and Day 3 (86% vs 44%;  $p=0.0312$ ), though it only reached statistical significance for Days 1 and 3 (Supplemental Figure 7A,  $n=6$  animals, Wilcoxon matched-pairs signed rank test, two tails). For 1 hour post-DBS, the induced crisis time on Day 0 decreased significantly on Day 1 (92% vs 61%;  $p=0.0156$ ), Day 2 (92% vs 64%;  $p=0.0156$ ), and Day 3 (93% vs 49%;  $p=0.0156$ ) (Supplemental Figure 7A,  $n=6$  animals, Wilcoxon matched-pairs signed rank test, two tails). Together, these results suggest that the iCNN pathway and CL interact to control the onset of dystonic crises, and that CL-DBS may provide prolonged and cumulative therapeutic effects for alleviating dystonic crises.

## Discussion

Little is known about iCNNS, and their functional contribution has been historically limited to motor learning and coordination (53–57). However, recent studies have increasingly supported a more prominent role for this subtype of cerebellar nuclei neurons, showing that they have distinct anatomical, electrophysiological, and protein expression properties (20, 21, 53) and that they may be involved in non-motor processes (58). For example, Judd et al. 2021 found that iCNNS restricted to the anterior interposed cerebellar nucleus send non-canonical, widespread projections to motor and non-motor areas (20). Our data suggest that iCNNS control the onset of dystonic crisis through their interaction with the CL. To our knowledge, this is the first evidence to support a role for iCNNS in disease, to describe a functional role for its extracerebellar projections outside the inferior olive, and to characterize its interaction with the motor network in disease. This finding of a precise, cell type-specific circuit may hold promise as a therapeutic avenue for intervention in patients with dystonic crisis or other refractory and debilitating forms of dystonia, with our data raising opportunities for further preclinical and clinical investigation. The significance of uncovering the distinct functions of intermingled neurons, like those of the cerebellar nuclei, has been highlighted in other brain areas and diseases. In a mouse model of Parkinson's disease, Spix et al. 2021 leveraged differences in cell-type specific neurons within the external globus pallidus to develop an optimized protocol for DBS, leading to longer-lasting therapeutic effects when compared to conventional DBS (22). Adapting this approach for optimizing DBS directed to iCNNS and its projections in the CL may yield similarly promising therapeutic results for patients with dystonia or other cerebellar-related disorders. Whether iCNNS contribute to other diseases remains an open question, although we anticipate that our results will encourage the further exploration of this possibility and the therapeutic utility of this understudied neuronal population. We found that DBS of the CL alleviated dystonic crises induced by iCNN photoactivation. While this result suggests that both structures interact to control the onset of dystonic crises, it does not reveal the exact nature of how this interaction occurs. Future studies are needed to investigate whether this therapeutic effect relies solely on the iCNN-CL projection, how iCNN activity modulates CL activity on a moment-to-moment basis during crisis induction, and how CL activity may further influence other connected motor structures beyond the basal ganglia. Elucidating these features may pinpoint the complete repertoire of neural substrates in the motor network that collaborate to induce dystonic crises and how they interact to drive the condition. Answering these questions may reveal critical disease-modifying therapeutic strategies.

Our study utilizes a unique intersectional genetic approach leveraging the developmental, *Ptf1a*-dependent expression of cre, which allowed access to iCNNS in all cerebellar nuclei. This may explain, at least in part, why our anatomical results may appear inconsistent with a recent study. Unlike our study, Judd et al. 2021 did not find that iCNNS project to the CL, which may be due to their viral injection strategy of cre-dependent fluorescent proteins in *Vgat-cre* mice (20). Specifically, the potential iCNNS that could be labeled with this technique were restricted primarily to the injected region (the anterior interposed cerebellar nucleus, a portion of one of three cerebellar nuclei) and dependent on the variability of targeting and viral expression, which may have not included those iCNNS that do project to the CL. In fact, we found CL-projecting iCNNS in all three cerebellar nuclei (Supplemental Figure 5 [↗](#)).

Our approach of leveraging the *Ptf1a*-specific expression of opsins in iCNNS and the anatomical restriction of their projections in the superior cerebellar peduncle provided an opportunity to selectively modulate their activity while avoiding unwanted photomodulation of nearby regions. While the robust ChR2-YFP expression in the targeted region of the superior cerebellar peduncle validated our approach, we cannot exclude the possibility that other observable nearby *Ptf1a*-expressing axons in the Kolliker-Fuse nucleus (KF), supratrigeminal nucleus (Su5), and motor trigeminal nucleus (Mo5) may have contributed to the optogenetically induced behaviors we observed (Supplemental Figure 2A [↗](#)). Similarly, *Ptf1a*-expressing projections from Purkinje cells in the parabrachial nucleus, which predominantly target areas around the superior cerebellar peduncle around 5.6 mm posterior to bregma, may have been photomodulated from our approach

(59). Nonetheless, this is unlikely as the light spread from our setup was calculated to not sufficiently illuminate these regions for photomodulation (see **Methods – optical fiber implantation and stimulation**); moreover, these regions are known to be involved in breathing, the sensorimotor control of the trigeminal nerve, and place preference, which would be unlikely drivers of dystonic crisis.

Although our experiments support a role for the iCNN pathway in controlling the onset of dystonic crisis, it is highly likely that excitatory cerebellar nuclei neurons also contribute to the condition as supported by studies into forms of paroxysmal dystonia. Wu et al. 2025 showed that selective photoactivation of excitatory cerebellar nuclei neurons induced dystonia-like movements in healthy mice, and that selective ablation of these neurons alleviated attacks in mouse models of paroxysmal dystonia (19). Other studies similarly supported a contribution for excitatory cerebellar nuclei in paroxysmal dystonia though their optogenetic methods technically did not exclude iCNNs from being manipulated in their studies. While iCNNs project outside the cerebellum and to the cerebellar cortex, they are also known to collateralize widely and form local synaptic connections with excitatory cerebellar nuclei neurons (17, 20, 53); thus, inhibitory and excitatory cerebellar nuclei neuron activity are tightly linked. Furthermore, Judd et al. 2021 showed that the excitatory and inhibitory cerebellar nuclei share many inputs and extracerebellar outputs (20), suggesting that they work synergistically. One possibility is that the excitatory neurons play a major role in the severity of baseline dystonia whereas the inhibitory neurons set the threshold for the dystonic crisis. While we cannot exclude the possibility that our optogenetic manipulation of iCNN activity through Chr2 could have caused backpropagation and influenced excitatory cerebellar nuclei neurons, it still does not discount our finding that direct manipulation of iCNN activity ultimately contributed to the phenotypes we observed in this study, regardless of what other structures may have been involved or required. Future studies are needed to investigate how the excitatory and cerebellar nuclei neurons interact to control dystonic crisis and other forms of dystonia, which may reveal population-specific strategies for designing therapeutic interventions to address the broader symptomology that collectively impact patients with dystonia.

## Materials and Methods

### Clinical methods

We performed a retrospective chart review of patients admitted to Texas Children's Hospital for the primary diagnosis of status dystonicus (also termed dystonic crisis) using (ICD9/10 codes) from 2015-2020 under approved IRB (H-48706). Demographics, medical history, and clinical notes were reviewed for all patients and information included etiology, laboratory studies, imaging, treatments, dosing, response, length of stay, and recurrence of symptoms. Efficacy of treatment was determined by patient/physician report as documented within the clinical notes.

### Animals

All experiments were performed following the relevant ethical regulations for animal testing. All mice were housed in an AALAS-accredited facility on a 14h/10h light/dark cycle. Mice of both sexes were studied. Husbandry, housing, euthanasia, and experimental guidelines were reviewed and approved by the Institutional Animal Care and Use Committee (IACUC) of Baylor College of Medicine (protocol number: AN-5996).

Dr Chris Wright (Vanderbilt University School of Medicine) kindly provided the *Ptf1a<sup>Cre</sup>* mice (30, 33). We purchased the *Vglut2<sup>floxed</sup>* (*Vglut2<sup>fx</sup>*, #012898) mice (60) from The Jackson Laboratory (Bar Harbor, ME, USA) that contained *LoxP* sites surrounding exon 2 of the gene encoding vesicular glutamate transporter 2 (VGLUT2). These two mouse lines were bred out as described previously to generate dystonic *Ptf1a<sup>Cre</sup>;Vglut2<sup>fx/fx</sup>* mice (30). To develop dystonic transgenic mice with restricted *Sun1* expression, we crossed these *Ptf1a<sup>Cre</sup>;Vglut2<sup>fx/fx</sup>* mice to heterozygous or homozygous *ROSA<sup>lox-stop-lox-Sun1</sup>*  $\lambda$  lines (*B6;129-Gt(ROSA)26Sor<sup>tm5(CAG-Sun1/sfGFP)Nat/J</sup>*, Strain #:021039, Jackson Laboratory, Bar Harbor, ME, USA). To gain light-sensitive control over inhibitory

cerebellar nuclei neurons with channelrhodopsin (ChR2) or archaerhodopsin (Arch), we crossed *Ptf1a<sup>Cre</sup>;Vglut2<sup>fx/fx</sup>* or *Ptf1a<sup>Cre</sup>* males to either *Ai32 ROSA<sup>lox-stop-lox-ChR2-EYFP</sup>* (B6;129-*Gt(ROSA)26Sor<sup>tm32(CAG-COP4\*H134R/EYFP)Hze/J</sup>*, Strain #:024109, Jackson Laboratory, Bar Harbor, ME) or *Ai40D (Gt(ROSA)<sub>26Sor</sub><sup>tm40.1(CAG-aop3/GFP)Hze/J</sup>*, Strain #:021188, Jackson Laboratory, Bar Harbor, ME) females(61). These genotypes of all offspring were confirmed by PCR of digested tissue (tail snips or ear punches) and confirmed by presence of Sun1-GFP, ChR2-EYFP, or Arch-EYFP signal in select neurons (it is important to ensure that cre-dependent expression is not present in all neurons, which would indicate germline transmission). For experimental studies, the day of birth was considered as postnatal day 0 (P0).

## Surgery

Surgery for awake optogenetics was performed as described previously (62). In brief, mice were anesthetized with 4% isoflurane in an induction chamber until unresponsive to the toe-pinch reflex. After transferring to a stereotaxic platform (David Kopf Instruments, Tujunga, CA, USA), isoflurane was lowered and maintained at 2% for the duration of surgery. Using aseptic technique and a sterile work field, the mouse was cleaned and prepped and the skin above the skull opened, and a small craniotomy of approximately 1 mm in diameter made above the target region(s). Following the implantation of optical fibers or deep brain stimulation electrodes as described below, all animals were allowed to recover for at least three days to a maximum of one week after surgery. The following surgical techniques were either employed as individual experiments or combined depending on the requirements of the experiment.

## Optical fiber implantation and stimulation

Optical fiber implant surgeries began as described above. One (for unilateral) or two (for bilateral) small craniotomies of about 1mm were performed dorsal to the target region through which optical fibers (Thorlabs, Newton, NJ, USA; #FT200UMT) were lowered into the target region: the superior cerebellar peduncle (5.02 mm posterior and  $\pm 1.25$  mm lateral to Bregma, 2.5 mm ventral from the brain surface). Optical fibers had been previously glued into ceramic ferrules (Thorlabs, Newton, NJ, USA; #CFLC230-10), polished (Thorlabs, Newton, NJ, USA; #LF5P, #LF3P, #LF1P, #LF03P, #LFCF), epoxied to each other at a set distance using Bondic, (a UV light-activated bonding agent; Bondic, Niagara Falls, NY, USA), and placed inside ceramic mating sleeves (Thorlabs, Newton, NJ, USA; #ADAL 1–5) prior to implantation. The optical fibers and 1-2 metal rods, used for holding the mouse's head stable while connecting the optical fiber patch cables, were affixed to the skull with C&B Metabond (Parkell, Inc., Edgewood, NY, USA, SKU: S380) and Teets 'Cold Cure' Dental Cement (A-M Systems, LLC, Carlsborg, WA, USA, Catalog #525000 and #526000).

Stimulation patterns were programmed and recorded using Spike2 software and delivered using a CED Power1401 data acquisition interface (CED, Cambridge, UK) to control a 470 nm LED (Thorlabs, Newton, NJ, USA; #M470F4) or a 561 nm laser (CrystaLaser, Reno, NV, USA; # CL561-050). Maximum LED power at the end of the implanted fiber was measured to be  $\sim 3.0$  mW and stimulation consisted of 50 Hz square pulses of blue 470 nm light. Maximum laser power at the end of the implanted fiber was measured to be  $\sim 10$  mW and stimulation consisted of a continuous pulse of green 561 nm light. The light powers were calculated to be capable of driving neurons at a distance of about 0.2 mm away or 0.4 mm away from the fiber tip for 470 nm LED light and 561 nm laser light, respectively, using the threshold of  $1 \text{ mW/mm}^2$  (63).

## Tracer injections

This procedure for tracer injections has been described in detail previously (64). Briefly, prior to surgery, the glass micropipettes (Borosilicate Standard Wall without Filament glass capillaries, 1.5 mm o.d.  $\times$  0.86 mm i.d.  $\times$  75 mm length) were prepared using a micropipette puller with the heat level set at 60 on the Step 1 setting of the Narishige PC-10 Puller and with two heavy weights and one light weight attached. Prior to use, the micropipette tips were clipped using forceps to ensure dispensability of neural tracer, the micropipette was attached to the Nanoject II, and  $\sim 1.0$  microliters of BDA 3k were loaded into the micropipette. Then, the surgery proceeded as described

above for the optical fiber implantation. Except, instead of optical fibers, the filled micropipette was lowered slowly into the stereotaxic coordinates for the centrolateral nucleus of the thalamus (1.50 mm posterior and  $\pm 0.80$  mm lateral to Bregma, 3.25 mm ventral from the brain surface). The Nanoject II was set to inject the smallest possible amount at the slowest available speed, and injections were given at 10 second intervals until  $\sim 75$  nL of BDA 3K were injected. After waiting five minutes, the micropipette was slowly taken out of the brain. The procedure was repeated for the contralateral site. After injections, the craniotomies were covered with antibiotic and the skull and skin were sealed with C&B Metabond (Parkell, Inc., Edgewood, NY, USA, SKU: S380) and Teets 'Cold Cure' Dental Cement (A-M Systems, LLC, Carlsborg, WA, USA, Catalog #525000 and #526000). Mice were transcardially perfused 9-12 days after the tracer injection procedure to allow the BDA 3K to penetrate neurons and travel retrogradely into the soma of input neurons (51, 52).

## DBS electrode implantation and stimulation

DBS electrode implant surgeries were performed exactly as the optical fiber implantation surgeries. Except, instead of optical fibers, custom 50 mm twisted bipolar Tungsten DBS electrodes were used (PlasticsOne, Roanoke, VA, USA; #8IMS303T3B01) and targeted to the centrolateral nucleus of the thalamus (1.50 mm posterior and  $\pm 0.78$  mm lateral to Bregma, 2.55 mm ventral from the brain surface). For bilateral implantation, the two electrodes were fixed together using Bondic, a UV light-activated bonding agent (Bondic, Niagara Falls, NY, USA). The electrodes and 1-2 metal rods, used for holding the mouse's head stable while connecting the DBS cables, were secured to the head with C&B Metabond (Parkell, Inc., Edgewood, NY, USA, SKU: S380) and Teets 'Cold Cure' Dental Cement (A-M Systems, LLC, Carlsborg, WA, USA, Catalog #525000 and #526000).

For DBS of the centrolateral nucleus of the thalamus, we used a Multichannel Systems Pulse generator (AMPI, Jerusalem, Israel) programmed to deliver 30  $\mu$ A, 60  $\mu$ s biphasic square pulses at 130 Hz.

## Behavioral analyses

The *Ptf1a<sup>Cre</sup>;Vglut2<sup>fx/fx</sup>* mutant mice exhibit dystonic symptoms of mild-to-moderate twisting postures in the limbs, trunk, head, and/or tail interrupted by random and intermittent attacks of generalized dystonia in several body parts reminiscent of dystonic crises (30). Similar to human patients in which the same underlying genetic mutation may result in a spectrum of dystonic symptoms across patients (34, 35), the severity of the underlying dystonic symptoms in the *Ptf1a<sup>Cre</sup>;Vglut2<sup>fx/fx</sup>* mouse can vary between animals. Spontaneous and optogenetically-induced dystonic crises were marked by prolonged and severe dystonic posturing including extended limbs, rigidity throughout the body, stiff tail, splayed digits, toppling over, and severely impaired ambulation for at least three seconds. Optogenetically-induced attacks persisted throughout the length of the optogenetic stimulation, except during or following DBS of the centrolateral nucleus of the thalamus.

The behavior of experimental mice in an open field was video recorded and video data from before and during stimulation were analyzed. For experiments involving photoinhibition (Figure 3B) and DBS of the CL (Figure 4G), three trials were given each day for four consecutive days. To detect potential changes in the incidence of dystonic crises, we measured the percentage of time that a mouse spent in a dystonic crisis during each period (before vs during stimulation), calculated the average for each period on a given day if applicable, and made statistical comparisons using the Wilcoxon matched-pairs signed rank test. Throughout this study, we define a dystonic crisis as observable dystonic muscle contractions or postures in at least two body parts in addition to severely limited ambulation for at least 3 seconds, a sufficient time to confidently determine that ambulation was limited (rather than due to resting) and a result of abnormal muscle activity.

For bilateral photoactivation of the superior cerebellar peduncle in *Ptf1a<sup>Cre</sup>;Vglut2<sup>fx/fx</sup>;ROSA<sup>Isl-Chr2/EYFP</sup>* mice, two-minute periods were video recorded before and during stimulation. For bilateral photoinhibition of the superior cerebellar peduncle in *Ptf1a<sup>Cre</sup>;Vglut2<sup>fx/fx</sup>;ROSA<sup>Isl-Arch/EYFP</sup>* mice, behavioral video data was collected over four consecutive days. To establish a

baseline for how much time the mice exhibit dystonic crises over a 35-minute session without optogenetic manipulation, we performed this experiment without any photostimulation on Day 0 (Figure 3B). To test whether photostimulation influenced the percentage of time spent in dystonic attack, video was recorded for five minutes before and five minutes during stimulation. To increase confidence that any behavioral change was a result of optogenetic manipulation, we repeated the stimulation paradigm three times on each day, resulting in a 35-minute session for each day (Figure 3B).

For unilateral photoactivation of the superior cerebellar peduncle and bilateral DBS of the CL in *Ptf1a<sup>Cre</sup>;Vglut2<sup>fx/fx</sup>;ROSA<sup>lsl-Chr2/EYFP</sup>* mice, we collected behavioral video data over four consecutive days. Each day consisted of an 86-minute session divided into five distinct periods: photobaseline, DBS period, immediately post-DBS, 30 minutes post-DBS, and 1 hour post-DBS (Figure 4G). During each distinct period, a 2-minute stimulation of blue light (470 nm light; 50 Hz square pulses;  $\geq 1$  mW at fiber tip) was administered followed by 2 minutes of no light stimulation. This paradigm was repeated three times for each distinct time period. The percentage of time spent in an attack was quantified for each of the three light pulses, and the average of these values was analyzed. To establish a baseline for how much time the mice spend in a dystonic crisis induced by iCNN photoactivation, we performed this experiment without any DBS on Day 0 (Figure 4G). DBS was administered on Days 1-3. DBS was only performed in the DBS period for 10 minutes (130 Hz, 60us, 30uA), starting with the onset of the first light pulse and ending with the offset of the third light pulse.

## Tissue processing and immunohistochemistry

Perfusion and tissue fixation were performed as previously described (65). In brief, mice were anesthetized with Avertin (2, 2, 2-Tribromoethanol, Sigma-Aldrich, St. Louis, MO, USA; #T48402) via intraperitoneal injection. Once mice were deeply anesthetized, a whole-body perfusion was performed first with ice-chilled 0.1M phosphate-buffered saline (PBS; pH 7.4), then with ice-chilled 4% paraformaldehyde (4% PFA) diluted in PBS. The brain was then dissected out and placed in 4% PFA for 24 to 48 hr for post-fixation at 4°C. Cryoprotection was then performed by placing the tissue in stepwise sucrose dilutions, first in 15% sucrose in PBS followed by 30% sucrose in PBS. Brains were stored at 4°C during stepwise sucrose incubation steps. After cryoprotection, the tissue was embedded in Tissue-Tek O.C.T. Compound (Sakura, Torrance, CA, USA) and frozen at -80°C. For immunohistochemistry, free-floating sections cut at 40um on the cryostat were incubated in antibodies in a solution of 10% normal goat or donkey serum and 0.01% Tween-20. For all stains, sections were blocked for 2 h with the blocking solution at room temperature and then incubated in primary antibodies overnight at room temperature. Sections were then washed with PBS 3 times for 5 min each and then incubated in secondary antibodies for 2 h. Sections were washed again 3 times in PBS for 5 min each and mounted onto slides. Slides with fluorescent signal were immediately cover-slipped using FluoroGel with Dapi as a medium. Antibodies used for immunohistochemistry (primary antibodies) were: GFP to visualize Chr2 and Sun1-GFP (Ch, Abcam, 1:1000), NeuroTrace fluorescent Nissl 530/615 to visualize neurons (Molecular Probes Inc, Eugene, OR, USA, #N21482; 1:1500), and Streptavidin Alexa Fluor 647 to visualize neurons filled with BDA 3K (Thermo Fisher Scientific, Eugene, OR, USA, #S21374); Secondary antibodies were: donkey anti-chicken secondary antibodies conjugated to 488 fluorophores (Invitrogen) diluted to 1:1500.

## *In situ* hybridization (ISH)

ISH was performed by the RNA ISH Core at Baylor College of Medicine using an automated robotic platform as described previously (66). ISH was used to visualize *Vglut2*, *Vgat*, and *YFP* expression in unfixed, fresh frozen tissue cut in 25  $\mu$ m-thick coronal brain sections. Digoxigenin (DIG)-labeled mRNA antisense probes against *Vglut2*, *Vgat*, and *YFP* were generated using reverse-transcribed mouse cDNA as a template and an RNA DIG-labeling kit from Roche. Primer and probe sequences for the *Vglut2*, *Vgat*, and *YFP* probes are available on the Allen Brain Atlas website (<http://www.brain-map.org>).

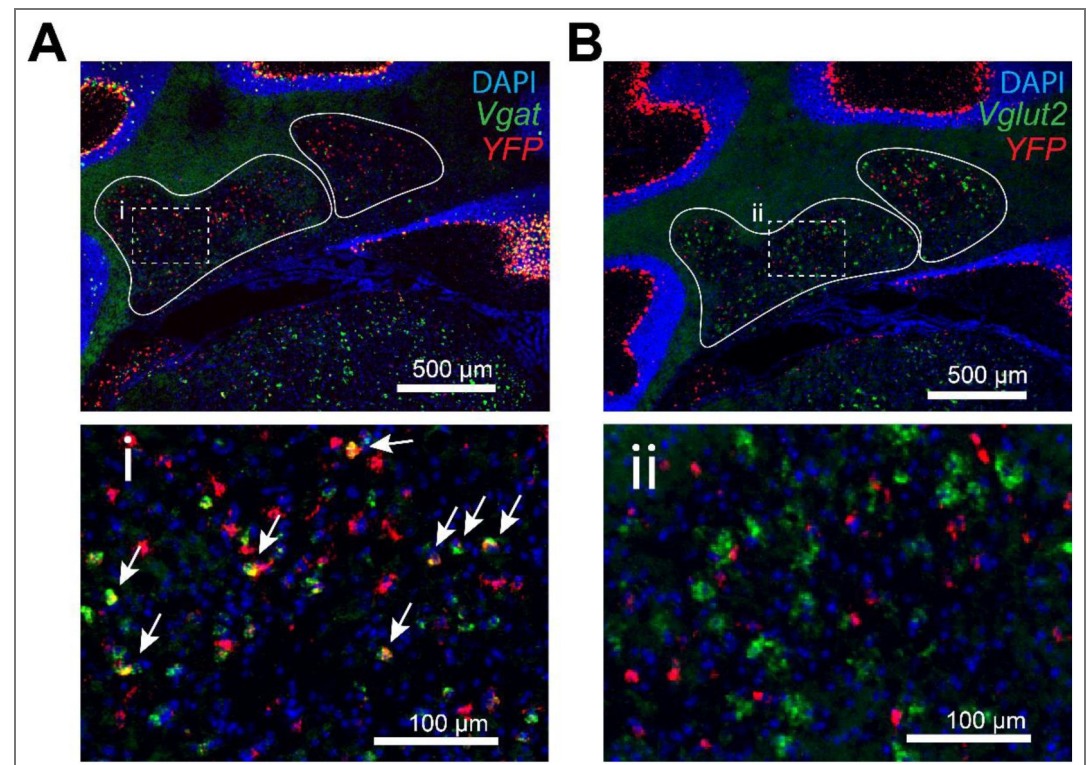
## Imaging of immunostained tissue sections

Photomicrographs of stained tissue sections were captured using either a Zeiss Axio Imager.M2 microscope equipped with Zeiss AxioCam MRm and MRc5 cameras (Zeiss, Oberkochen, Germany) or a Leica DM4000 B LED microscope equipped with Leica DFC365 FX and Leica DMC 2900 cameras (Leica Microsystems Inc, Wetzlar, Germany). Zeiss Zen software was used for image acquisition from the Zeiss microscope. Leica Application Suite X (LAS X) software was used for image acquisition from the Leica microscope. Images were corrected for brightness and contrast using Adobe Photoshop CS5 (Adobe Systems, San Jose, CA, USA) for figure preparation. Schematics were made in Adobe Illustrator CC.

## Data analysis and statistics

Data are presented as mean±s.e.m. and were analyzed with a Wilcoxon matched-pairs signed rank test (non-normally distributed data with unequal variance). For all statistical tests,  $P < 0.05$  was considered as statistically significant. All statistical analyses were performed using GraphPad Prism (GraphPad Software, La Jolla, CA, USA) software.

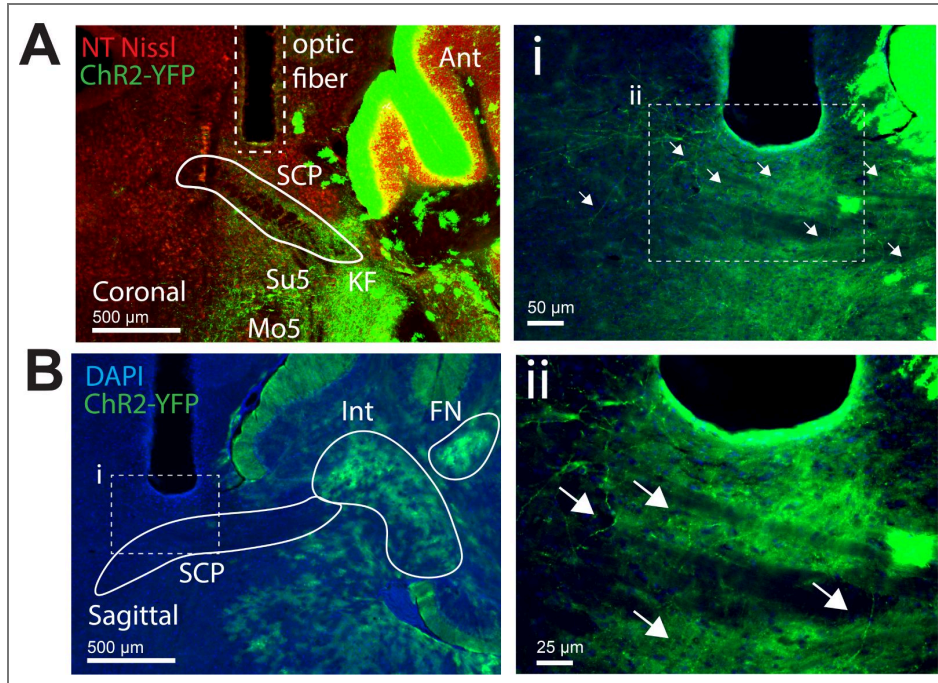
## Figure supplements



**Supplemental Figure 1. Ptf1a-cre induced expression of cre-dependent ChR2-YFP in inhibitory cerebellar nuclei neurons, but not excitatory cerebellar nuclei neurons, in *Ptf1a<sup>Cre</sup>;Vglut2<sup>fx/fx</sup>;ROSA<sup>Isl-Chr2/EYFP</sup>* mice.** (A) *In situ* hybridization in a coronal section showing mRNA expression *Vgat* and *YFP* as well as DAPI staining ( $n=3$  animals; 3 sections per animal). The cerebellar nuclei are outlined in white. Inset (i) is a higher magnification image from (A) with white arrows marking cerebellar nuclei neurons that were co-labeled with *Vgat* and *YFP* probes. (B) *In situ* hybridization in a coronal section showing mRNA expression *Vglut2* and *YFP* as well as DAPI, with the cerebellar nuclei outlined in white ( $n=3$  animals; 3 sections per animal). Inset (ii) is a higher magnification image of (B) showing that there was no co-labeling of *Vglut2* and *YFP*.

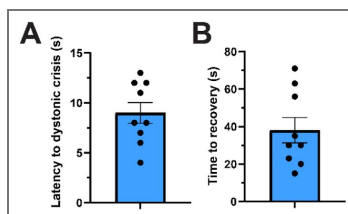
**Supplemental Figure 2. Anatomical verification of optical fibers over the superior cerebellar peduncle (SCP), which houses extracerebellar projections from inhibitory cerebellar nuclei neurons as labeled with Chr2-YFP in *Ptf1a<sup>Cre</sup>;Vglut2<sup>fx/fx</sup>;ROSA<sup>Isl-Chr2/EYFP</sup>* mice.**

(A) Coronal section demonstrating location of optic fiber over the SCP (n=9 animals, 3 sections per animal). Note the punctate labeling of axonal projections expressing Chr2-YFP in the SCP. (B) Sagittal section demonstrating location of optic fiber over the SCP (n=3 animals, 3 sections per animal). Insets (i and ii) show higher magnification of the SCP from (B), highlighting the expression of Chr2-YFP in axonal projections with white arrows. SCP, superior cerebellar peduncle; Ant, anterior cerebellar lobe; KF, Kolliker-Fuse nucleus; Su5, supratrigeminal nucleus; Mo5, trigeminal motor nucleus; Int, interposed cerebellar nucleus; FN, fastigial cerebellar nucleus.



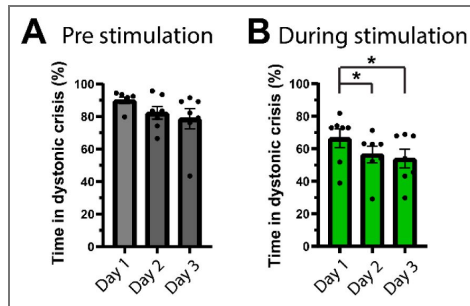
**Supplemental Figure 3. Photoactivation of the inhibitory cerebellar nuclei neuron pathway through the superior cerebellar peduncle induced dystonic crises that occurred within a short latency from light onset and that persisted many seconds after stimulation ends in *Ptf1a<sup>Cre</sup>;Vglut2<sup>fx/fx</sup>;ROSA<sup>Isl-Chr2/EYFP</sup>* mice.**

(A) Dystonic crises were induced at around 10 seconds from light onset. (B) After the light stimulation ends, the induced dystonic crisis persisted for around 40 seconds. n=9 animals.



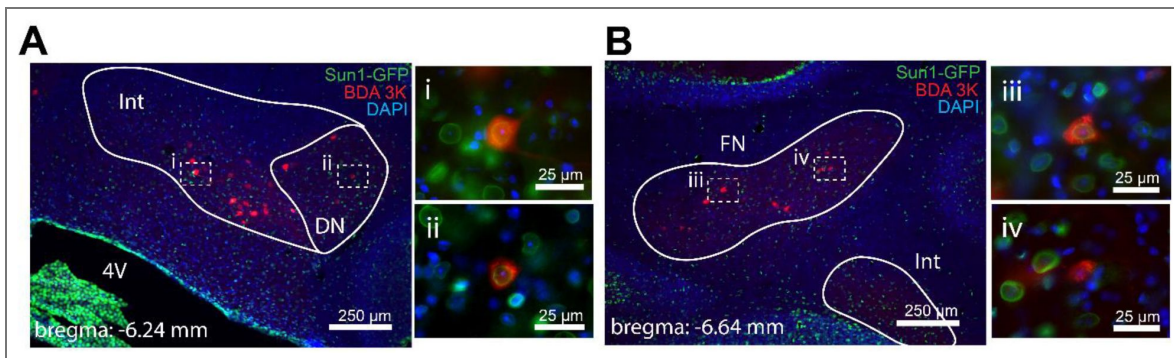
**Supplemental Figure 4. Photostimulation over several days resulted in a reduction in the time spent in dystonic crisis.**

(A) For the pre stimulation periods when comparing Day 1 (the first day of stimulation) against Day 2 ( $p=0.0625$ ) and Day 3 ( $p=0.0781$ ), there was a trend toward a reduction in dystonic crisis, but it was not statistically significant. (B) For the during stimulation periods, there was a significant reduction in dystonic crises when comparing Day 1 to Day 2 ( $p=0.0312$ ) and Day 3 ( $p=0.0156$ ). For all statistics,  $n=7$  animals, Wilcoxon matched-pairs signed rank test, two tailed.



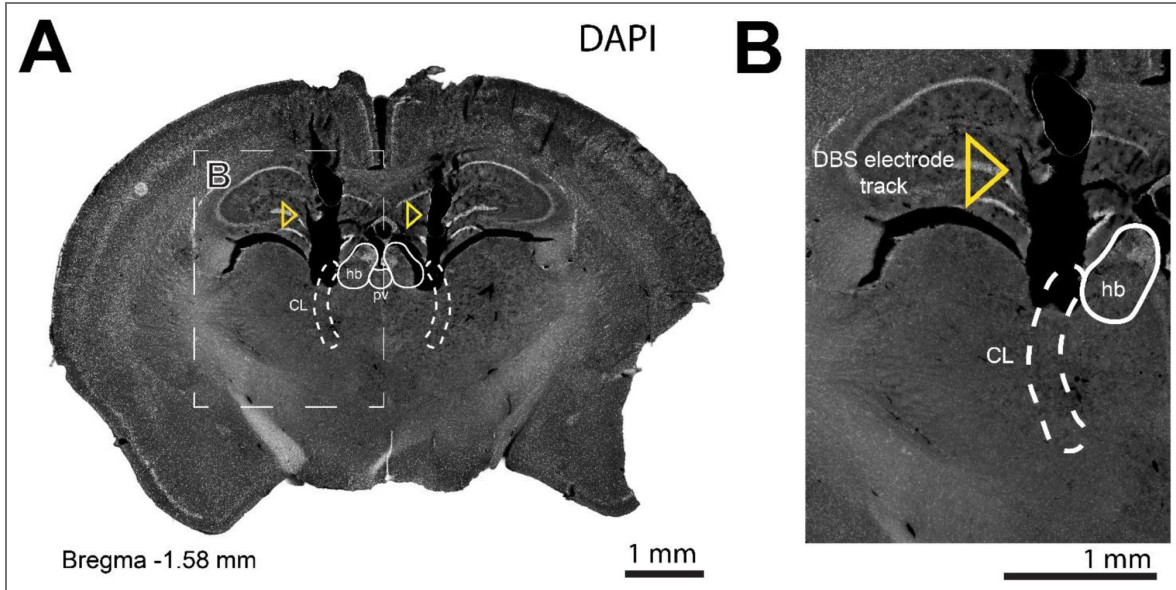
**Supplemental Figure 5. Inhibitory cerebellar nuclei neurons from all three major cerebellar nuclei (fastigial, interposed, dentate) project to the centrolateral nucleus of the thalamus ( $n=4$  animals, 3 sections per animal).**

(A) Coronal section showing that neurons from the interposed and dentate cerebellar nucleus were filled with BDA 3K following injection of BDA 3K, a predominantly retrograde tracer, in the centrolateral nucleus of the thalamus. Insets (i) and (ii) are higher magnification images of (A) showing the co-labeling of DAPI, Sun1-GFP, and BDA 3K in the interposed and dentate cerebellar nucleus, respectively. (B) Coronal section showing that neurons from the fastigial cerebellar nucleus were filled with BDA 3K following injection of BDA 3K, a predominantly retrograde tracer, in the centrolateral nucleus of the thalamus. Inset (iii) is a higher magnification image of (B) showing a co-labeling of DAPI, Sun1-GFP, and BDA 3K. Inset (iv) is a higher magnification image of (B) showing co-labeling of DAPI and BDA 3K, but not Sun1-GFP. Int, interposed cerebellar nucleus; DN, dentate cerebellar nucleus; FN, fastigial cerebellar nucleus; 4V, fourth ventricle.



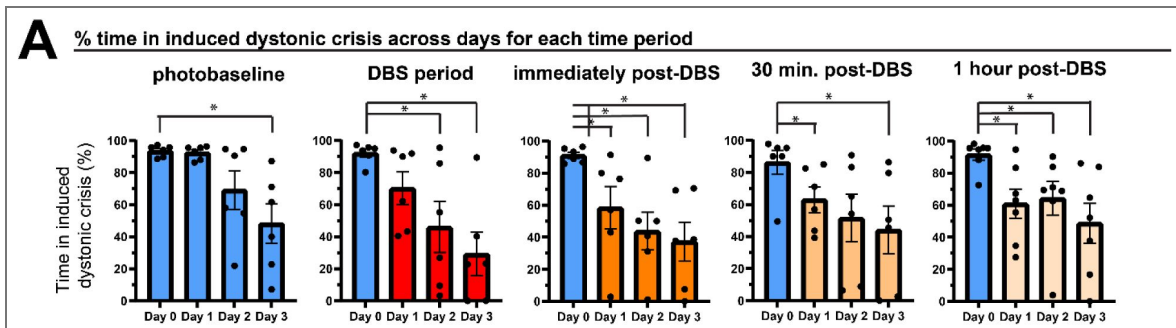
**Supplemental Figure 6. Anatomical verification of the surgical targeting of deep brain stimulation electrodes in the centrolateral nucleus of the thalamus.**

(A) Immunohistochemical staining of DAPI showing the tracks formed by the bilateral implantation of deep brain stimulation electrodes in the centrolateral nucleus of the thalamus (n=6 animals, 3 sections per animal). Yellow triangles mark the tracks formed by the DBS electrodes above and with some penetration into the centrolateral nucleus of the thalamus. (B) Inset of A showing a higher magnified image of the DBS electrode track in the centrolateral nucleus of the thalamus. CL, centrolateral nucleus of the thalamus; hb, habenula; pv, paraventricular thalamic nucleus.



**Supplemental Figure 7. Deep brain stimulation of the centrolateral nucleus of the thalamus over several days reduced the time in dystonic crises induced by photoactivation of the inhibitory cerebellar nuclei neuron pathway.**

(A) Comparing the induced dystonic crises during photobaseline on Day 0 against Day 3 revealed a significant reduction in dystonic crises ( $p=0.0312$ ). Photoinduced dystonic crises during DBS on Day 0 were reduced on Day 2 ( $p=0.0312$ ) and Day 3 ( $p=0.0312$ ). Photoinduced dystonic crises immediately post-DBS on Day 0 were decreased on Day 1 ( $p=0.0312$ ), Day 2 ( $p=0.0312$ ), and Day 3 ( $p=0.0312$ ). For 30 minutes post-DBS, photoinduced crises were reduced on Day 1 ( $p=0.0312$ ) and Day 3 ( $p=0.0312$ ). For 1 hour post-DBS, photoinduced crises decreased on Day 1 ( $p=0.0156$ ), Day 2 ( $p=0.0156$ ), and Day 3 ( $p=0.0156$ ). For all statistics: n=6 animals, Wilcoxon matched-pairs signed rank test, two-tailed, error bars are defined as standard error of the mean.



## Data availability

All data, code, and materials are available in the main text, supplementary materials, or available upon request to the corresponding author.

## Additional information

### Funding

Baylor College of Medicine Texas Children’s Hospital

The Jan and Dan Duncan Neurological Research Institute (Texas Children’s Hospital Duncan NRI)

The National Institute of Neurological Disorders and Stroke grants R01NS119301 and R01NS127435 (RVS) The National Institute of Neurological Disorders and Stroke grant K08NS121600 (JSG)

Eunice Kennedy Shriver National Institute of Child Health and Human Development of the National Institutes of Health under Award Number P50HD103555 for use of the Cell and Tissue Pathogenesis Core and In Situ Hybridization Core (the BCM IDDRC) (RVS)

The Ting Tsung and Wei Fong Chao Foundation (RVS)

The content is solely the responsibility of the authors and does not necessarily represent the official views of the National Center for Research Resources or the National Institutes of Health.

### Contributions

Conceptualization: AGRH, and RVS

Methodology: AGRH, MPD, JSG, MH, and RVS

Software: AGRH, MPD

Validation: AGRH, MPD

Formal analyses: AGRH, MPD

Investigation: AGRH, MPD, JSG, JEA, KAC, MH, and RVS

Data curation: AGRH, MPD, JSG, KAC, MH

Writing—original draft: AGRH, MPD, RVS

Writing—review & editing: AGRH, MPD, JSG, JEA, KAC, MH, and RVS

Visualization: AGRH, MPD, JSG, KAC, MH, and RVS

Supervision: RVS

Project administration: AGRH, MPD, JSG, KAC, MH, and RVS

Funding acquisition: JSG and RVS

### Funding

Funder	Grant reference number	Author
Baylor College of Medicine (BCM)		Roy V Sillitoe
Texas Children's Hospital (TCH)		Roy V Sillitoe
The Jan and Dan Duncan Neurological Institute		Roy V Sillitoe
The National Institute of Neurological Disorders and Stroke	R01NS119301	Roy V Sillitoe
The National Institute of Neurological Disorders and Stroke	R01NS127435	Roy V Sillitoe
The National Institute of Neurological Disorders and Stroke	K08NS121600	Jason S Gill

Eunice Kennedy Shriver National Institute of  
Child Health and Human Development of the P50HD103555  
National Institutes of Health

Roy V Sillitoe


The Ting Tsung and Wei Fong Chao  
Foundation


Roy V Sillitoe


## Author ORCID iDs


**Roy V Sillitoe:**  <https://orcid.org/0000-0002-6177-6190>


## Additional files

**Supplementary Movie 1.**  Movie of a patient in dystonic crisis at the hospital that was included in the study. The patient exhibits the debilitating dystonic postures characteristic of dystonic crisis including rigidity and stiffness in the neck, arms, fingers, and toes.

**Supplementary Movie 2.**  Movie of a *Ptf1a<sup>Cre</sup>;Vglut2<sup>fx/fx</sup>;ROSA<sup>Isl-Chr2/EYFP</sup>* mouse before, during, and after photoactivation of the inhibitory cerebellar nuclei neuron pathway via the superior cerebellar peduncle. A dystonic crisis was induced within several seconds of light onset, and the crisis persisted for many seconds after the end of light stimulation.

**Supplementary Movie 3.**  Movie of a *Ptf1a<sup>Cre</sup>;ROSA<sup>Isl-Chr2/EYFP</sup>* mouse before, during, and after photoactivation of the inhibitory cerebellar nuclei neuron pathway via the superior cerebellar peduncle. Although no dystonic crisis was induced, the animal moved abnormally with slowed movement, mild dystonia-like muscle tension, crawling, widened hind legs, dragging of the trunk, clunky locomotion, and wide steps.

**Supplementary Movie 4.**  Movie of a *Ptf1a<sup>Cre</sup>;Vglut2<sup>fx/fx</sup>;ROSA<sup>Isl-Arch/EYFP</sup>* mouse before and during photoinhibition of the inhibitory cerebellar nuclei neuron pathway via the superior cerebellar peduncle on Day 1 and Day 3 of photostimulation. The first half of the video consisted of footage from Day 1 of stimulation where there was a notable alleviation of the spontaneous dystonic crisis and restoration of mobility. On Day 3 of stimulation as shown in the second half of the video, the baseline time spent in spontaneous dystonic crisis was slightly less severe than Day 1, and photostimulation further improved the mobility of the dystonic mouse to a level that was better than that seen on Day 1 during photostimulation.

**Supplementary Movie 5.**  Movie of a *Ptf1a<sup>Cre</sup>;Vglut2<sup>fx/fx</sup>;ROSA<sup>Isl-Chr2/EYFP</sup>* mouse on Day 1 and Day 3 of deep brain stimulation (DBS) in the centrolateral nucleus of the thalamus (CL) showing the short-term and long-term therapeutic effects of DBS on dystonic crises induced by iCNN photoactivation. On Day 1, the photobaseline shows that photoactivation of the iCNN pathway via the superior cerebellar peduncle reliably induced a dystonic crisis; however, when DBS of the CL was administered concurrently with the light stimulation in the “during DBS” period, a dystonic crisis was induced only briefly and then the mouse quickly recovered its mobility. On Day 3, the photobaseline period shows that iCNN photoactivation still reliably induced dystonic crisis; however, concurrent DBS of the CL in the “during DBS” period prevented the occurrence of a dystonic crisis induced by iCNN photoactivation.

## References

1. Albanese A, Bhatia KP, Fung VSC, Hallett M, Jankovic J, Klein C, Krauss JK, Lang AE, Mink JW, Pandey S, *et al.* (2025) Definition and classification of dystonia. *Mov Disord* **40**:1248-1259 <https://doi.org/10.1002/mds.30220> | PubMed
2. Lumsden DE, King MD, Allen NM (2017) Status dystonicus in childhood. *Curr. Opin. Pediatr* **29**:674-682 <https://doi.org/10.1097/mop.0000000000000556> | PubMed
3. Fasano A, Ricciardi L, Bentivoglio AR, Canavese C, Zorzi G, Petrovic I, Kresojevic N, Kostić VS, Svetel M, Kovacs N, *et al.* (2012) Status dystonicus: predictors of outcome and progression patterns of underlying disease. *Mov Disord* **27**:783-788 <https://doi.org/10.1002/mds.24981> | PubMed

4. Saini AG, Hassan I, Sharma K, Muralidharan J, Dhawan S, Saini L, Suthar R, Sahu J, Sankhyan N, Singhi P (2022) Status Dystonicus in Children: A Cross-Sectional Study and Review of Literature. *J. Child Neurol* **37**:441-450 <https://doi.org/10.1177/08830738221081593> | PubMed
5. Garone G, Graziola F, Nicita F, Frascarelli F, Randi F, Zazza M, Cantonetti L, Cossu S, Marras CE, Capuano A (2020) Prestatus and status dystonicus in children and adolescents. *Dev. Med. Child Neurol* **62**:742-749 <https://doi.org/10.1111/dmcn.14425> | PubMed
6. Vogt LM, Yang K, Tse G, Quiroz V, Zaman Z, Wang L, Srouji R, Tam A, Estrella E, Manzi S, et al. (2024) Recommendations for the management of initial and refractory pediatric status dystonicus. *Mov Disord* **39**:1435-1445 <https://doi.org/10.1002/mds.29794> | PubMed
7. Sobstyl MR, Sławek JW, Ząbek M (2014) The neurosurgical treatment of patients in dystonic state - overview of the literature. *Neurol. Neurochir. Pol* **48**:63-70 <https://doi.org/10.1016/j.pjnns.2013.04.002> | PubMed
8. Marsden CD, Marion MH, Quinn N (1984) The treatment of severe dystonia in children and adults. *J. Neurol. Neurosurg. Psychiatr* **47**:1166-1173 <https://doi.org/10.1136/jnnp.47.11.1166> | PubMed
9. Quartarone A, Ruge D (2018) How many types of dystonia? pathophysiological considerations. *Front Neurol* **9** <https://doi.org/10.3389/fneur.2018.00012> | PubMed
10. Hallett M (2011) Neurophysiology of dystonia: The role of inhibition. *Neurobiol. Dis* **42**:177-184 <https://doi.org/10.1016/j.nbd.2010.08.025> | PubMed
11. Balachandar A, Vogt LM, Mithani K, Coleman SC, Ebden M, Leblanc-Miller A, Breitbart S, Fasano A, Gorodetsky C, Ibrahim GM (2025) Status dystonicus is a distinct state characterized by pallidal beta-band activity. *Nat. Commun* **16**:9352 <https://doi.org/10.1038/s41467-025-64416-9> | PubMed
12. Termsarasab P, Frucht SJ (2017) Dystonic storm: a practical clinical and video review. *J. Clin. Mov. Disord* **4** <https://doi.org/10.1186/s40734-017-0057-z> | PubMed
13. Lumsden DE, Cif L, Capuano A, Allen NM (2023) The changing face of reported status dystonicus - A systematic review. *Parkinsonism Relat Disord* **112** <https://doi.org/10.1016/j.parkreldis.2023.105438> | PubMed
14. Volpe JJ (2009) Cerebellum of the premature infant: rapidly developing, vulnerable, clinically important. *J. Child Neurol* **24**:1085-1104 <https://doi.org/10.1177/0883073809338067> | PubMed
15. Qin Y, Li Y, Sun B, He H, Peng R, Zhang T, Li J, Luo C, Sun C, Yao D (2018) Functional Connectivity Alterations in Children with Spastic and Dyskinetic Cerebral Palsy. *Neural Plast* **7058953** <https://doi.org/10.1155/2018/7058953> | PubMed
16. Sathyanesan A, Zhou J, Scafidi J, Heck DH, Sillitoe RV, Gallo V (2019) Emerging connections between cerebellar development, behaviour and complex brain disorders. *Nat. Rev. Neurosci* **20**:298-313 <https://doi.org/10.1038/s41583-019-0152-2> | PubMed
17. Keschull JM, Casoni F, Consalez GG, Goldowitz D, Hawkes R, Ruigrok TJH, Schilling K, Wingate R, Wu J, Yeung J, et al. (2024) Cerebellum Lecture: the Cerebellar Nuclei-Core of the Cerebellum. *Cerebellum* **23**:620-677 <https://doi.org/10.1007/s12311-022-01506-0> | PubMed
18. Nguyen MX, Brown AM, Lin T, Sillitoe RV, Gill JS (2025) Thalamic deep brain stimulation improves movement in a cerebellar model of lesion-based status dystonicus. *Neurotherapeutics* **22**:e00543 <https://doi.org/10.1016/j.neurot.2025.e00543> | PubMed
19. Wu X.-M, Lu B, He J.-Y, Zhang Y.-X, Wu Z.-Y, Xiong Z.-Q (2025) Aberrant outputs of glutamatergic neurons in deep cerebellar nuclei mediate dystonic movements. *Sci. Adv* **11**:eadp2377 <https://doi.org/10.1126/sciadv.adp2377> | PubMed
20. Judd EN, Lewis SM, Person AL (2021) Diverse inhibitory projections from the cerebellar interposed nucleus. *eLife* **10** <https://doi.org/10.7554/eLife.66231> | PubMed
21. Keschull JM, Richman EB, Ringach N, Friedmann D, Albarran E, Kolluru SS, Jones RC, Allen WE, Wang Y, Cho SW, et al. (2020) Cerebellar nuclei evolved by repeatedly duplicating a conserved cell-type set. *Science* **370** <https://doi.org/10.1126/science.abd5059> | PubMed

22. Spix TA, Nanivadekar S, Toong N, Kaplow IM, Isett BR, Goksen Y, Pfenning AR, Gittis AH (2021) Population-specific neuromodulation prolongs therapeutic benefits of deep brain stimulation. *Science* **374**:201-206 <https://doi.org/10.1126/science.abi7852> | [PubMed](#)
23. Hernandez-Martin E, Vidmark JSL, MacLean JA, Sanger TD (2023) What is the effect of benzodiazepines on deep brain activity? A study in pediatric patients with dystonia. *Front. Neurol* **14** <https://doi.org/10.3389/fneur.2023.1215572> | [PubMed](#)
24. Spay C, Albares M, Lio G, Thobois S, Broussolle E, Lau B, Ballanger B, Boulinguez P (2018) Clonidine modulates the activity of the subthalamic-supplementary motor loop: evidence from a pharmacological study combining deep brain stimulation and electroencephalography recordings in Parkinsonian patients. *J. Neurochem* **146**:333-347 <https://doi.org/10.1111/jnc.14447> | [PubMed](#)
25. Rotter A, Frosthalm A (1988) Cerebellar benzodiazepine receptors: cellular localization and consequences of neurological mutations in mice. *Brain Res* **444**:133-146 [https://doi.org/10.1016/0006-8993\(88\)90920-1](https://doi.org/10.1016/0006-8993(88)90920-1) | [PubMed](#)
26. Somogyi P, Takagi H, Richards JG, Mohler H (1989) Subcellular localization of benzodiazepine/GABAA receptors in the cerebellum of rat, cat, and monkey using monoclonal antibodies. *J. Neurosci* **9**:2197-2209 <https://doi.org/10.1523/jneurosci.09-06-02197.1989> | [PubMed](#)
27. Di Mauro M, Li Volsi G, Licata F (2013) Noradrenergic control of neuronal firing in cerebellar nuclei: modulation of GABA responses. *Cerebellum* **12**:350-361 <https://doi.org/10.1007/s12311-012-0422-2> | [PubMed](#)
28. Kim JE, Chae S, Kim S, Jung Y.-J, Kang M.-G, Heo WD, Kim D (2021) Cerebellar 5HT-2A receptor mediates stress-induced onset of dystonia. *Sci. Adv* **7** <https://doi.org/10.1126/sciadv.abb5735> | [PubMed](#)
29. Meijer IA, Fasano A (2022) Movement disorder emergencies: diagnosis and treatment. In: Frucht SJ (Ed). *Current Clinical Neurology* Springer International Publishing, Cham. pp. 183-199
30. White JJ, Sillitoe RV (2017) Genetic silencing of olivocerebellar synapses causes dystonia-like behaviour in mice. *Nat. Commun* **8** <https://doi.org/10.1038/ncomms14912> | [PubMed](#)
31. Brown AM, van der Heijden ME, Jinnah HA, Sillitoe RV (2023) Cerebellar dysfunction as a source of dystonic phenotypes in mice. *Cerebellum* **22**:719-729 <https://doi.org/10.1007/s12311-022-01441-0> | [PubMed](#)
32. Yamada M, Terao M, Terashima T, Fujiyama T, Kawaguchi Y, Nabeshima Y, Hoshino M (2007) Origin of climbing fiber neurons and their developmental dependence on Ptf1a. *J. Neurosci* **27**:10924-10934 <https://doi.org/10.1523/jneurosci.1423-07.2007> | [PubMed](#)
33. Hoshino M, Nakamura S, Mori K, Kawauchi T, Terao M, Nishimura YV, Fukuda A, Fuse T, Matsuo N, Sone M, et al. (2005) Ptf1a, a bHLH transcriptional gene, defines GABAergic neuronal fates in cerebellum. *Neuron* **47**:201-213 <https://doi.org/10.1016/j.neuron.2005.06.007> | [PubMed](#)
34. Argyelan M, Carbon M, Niethammer M, Ulug AM, Voss HU, Bressman SB, Dhawan V, Eidelberg D (2009) Cerebellothalamocortical connectivity regulates penetrance in dystonia. *J. Neurosci* **29**:9740-9747 <https://doi.org/10.1523/jneurosci.2300-09.2009> | [PubMed](#)
35. Kostić VS, Svetel M, Kabacki K, Ristić A, Petrović I, Schüle B, Kock N, Djarmati A, Romac S, Klein C (2006) Intrafamilial phenotypic and genetic heterogeneity of dystonia. *J. Neurol. Sci* **250**:92-96 <https://doi.org/10.1016/j.jns.2006.07.010> | [PubMed](#)
36. Lin S, Li N, Shu Y, Wang T, Huang P, Pan Y, Sun B, Zhang C, Li D, Wu Y (2024) Superior cerebellar peduncle deep brain stimulation for cerebral palsy. *J. Neurosurg* **141**:1407-1417 <https://doi.org/10.3171/2024.2.jns232471> | [PubMed](#)
37. Horisawa S, Arai T, Suzuki N, Kawamata T, Taira T (2019) The striking effects of deep cerebellar stimulation on generalized fixed dystonia: case report. *J. Neurosurg* **132**:712-716 <https://doi.org/10.3171/2018.11.JNS182180> | [PubMed](#)
38. Ruge D, Tisch S, Hariz MI, Zrinzo L, Bhatia KP, Quinn NP, Jahanshahi M, Limousin P, Rothwell JC (2011) Deep brain stimulation effects in dystonia: time course of electrophysiological changes in early treatment. *Mov Disord* **26**:1913-1921 <https://doi.org/10.1002/mds.23731> | [PubMed](#)

39. Reese R, Volkman J (2017) Deep brain stimulation for the dystonias: evidence, knowledge gaps, and practical considerations. *Mov Disord Clin Pract* **4**:486-494 <https://doi.org/10.1002/mdc3.12519> | PubMed
40. Lozano AM, Lipsman N, Bergman H, Brown P, Chabardes S, Chang JW, Matthews K, McIntyre CC, Schlaepfer TE, Schulder M, et al. (2019) Deep brain stimulation: current challenges and future directions. *Nat. Rev. Neurol* **15**:148-160 <https://doi.org/10.1038/s41582-018-0128-2> | PubMed
41. Cif L, Ruge D, Gonzalez V, Limousin P, Vasques X, Hariz MI, Rothwell J, Coubes P (2013) The influence of deep brain stimulation intensity and duration on symptoms evolution in an OFF stimulation dystonia study. *Brain Stimulat* **6**:500-505 <https://doi.org/10.1016/j.brs.2012.09.005> | PubMed
42. Jinnah HA, Neychev V, Hess EJ (2017) The anatomical basis for dystonia: the motor network model. *Tremor Other Hyperkinet Mov* **7** <https://doi.org/10.7916/d8v69x3s> | PubMed
43. Sondergaard RE (2023) Characterizing the cerebello-thalamo-cortical tracts in the pathophysiology of adult-onset idiopathic dystonia. *Graduate Studies* <https://doi.org/10.11575/prism/41566>
44. Tewari A, Fremont R, Khodakhah K (2017) It's not just the basal ganglia: Cerebellum as a target for dystonia therapeutics. *Mov Disord* **32**:1537-1545 <https://doi.org/10.1002/mds.27123> | PubMed
45. Bostan AC, Strick PL (2018) The basal ganglia and the cerebellum: nodes in an integrated network. *Nat. Rev. Neurosci* **19**:338-350 <https://doi.org/10.1038/s41583-018-0002-7> | PubMed
46. Calderon DP, Fremont R, Kraenzlin F, Khodakhah K (2011) The neural substrates of rapid-onset Dystonia-Parkinsonism. *Nat. Neurosci* **14**:357-365 <https://doi.org/10.1038/nn.2753> | PubMed
47. Uluğ AM, Vo A, Argyelan M, Tanabe L, Schiffer WK, Dewey S, Dauer WT, Eidelberg D (2011) Cerebellothalamocortical pathway abnormalities in torsinA DYT1 knock-in mice. *Proc Natl Acad Sci USA* **108**:6638-6643 <https://doi.org/10.1073/pnas.1016445108> | PubMed
48. Hoshi E, Tremblay L, Féger J, Carras PL, Strick PL (2005) The cerebellum communicates with the basal ganglia. *Nat. Neurosci* **8**:1491-1493 <https://doi.org/10.1038/nn1544> | PubMed
49. Chen CH, Fremont R, Arteaga-Bracho EE, Khodakhah K (2014) Short latency cerebellar modulation of the basal ganglia. *Nat. Neurosci* **17**:1767-1775 <https://doi.org/10.1038/nn.3868> | PubMed
50. Gornati SV, Schäfer CB, Eelkman Rooda OHJ, Nigg AL, De Zeeuw CI, Hoebeek FE (2018) Differentiating cerebellar impact on thalamic nuclei. *Cell Rep* **23**:2690-2704 <https://doi.org/10.1016/j.celrep.2018.04.098> | PubMed
51. Reiner A, Veenman CL, Medina L, Jiao Y, Del Mar N, Honig MG (2000) Pathway tracing using biotinylated dextran amines. *J. Neurosci. Methods* **103**:23-37 [https://doi.org/10.1016/s0165-0270\(00\)00293-4](https://doi.org/10.1016/s0165-0270(00)00293-4) | PubMed
52. Zhang W, Xu D, Cui J, Jing X, Xu N, Liu J, Bai W (2017) Anterograde and retrograde tracing with high molecular weight biotinylated dextran amine through thalamocortical and corticothalamic pathways. *Microsc Res Tech* **80**:260-266 <https://doi.org/10.1002/jemt.22797> | PubMed
53. Uusisaari M, Obata K, Knöpfel T (2007) Morphological and electrophysiological properties of GABAergic and non-GABAergic cells in the deep cerebellar nuclei. *J. Neurophysiol* **97**:901-911 <https://doi.org/10.1152/jn.00974.2006> | PubMed
54. Lefler Y, Yarom Y, Uusisaari MY (2014) Cerebellar inhibitory input to the inferior olive decreases electrical coupling and blocks subthreshold oscillations. *Neuron* **81**:1389-1400 <https://doi.org/10.1016/j.neuron.2014.02.032> | PubMed
55. Rasmussen A, Hesslow G (2014) Feedback control of learning by the cerebello-olivary pathway. *Prog. Brain Res* **210**:103-119 <https://doi.org/10.1016/b978-0-444-63356-9.00005-4> | PubMed
56. Bengtsson F, Hesslow G (2006) Cerebellar control of the inferior olive. *Cerebellum* **5**:7-14 <https://doi.org/10.1080/14734220500462757> | PubMed
57. Kim OA, Ohmae S, Medina JF (2020) A cerebello-olivary signal for negative prediction error is sufficient to cause extinction of associative motor learning. *Nat. Neurosci* **23**:1550-1554 <https://doi.org/10.1038/s41593-020-00732-1> | PubMed

58. van der Heijden ME, Rey Hipolito AG, Kim LH, Kizek DJ, Perez RM, Lin T, Sillitoe RV (2023) Glutamatergic cerebellar neurons differentially contribute to the acquisition of motor and social behaviors. *Nat. Commun* **14**:2771 <https://doi.org/10.1038/s41467-023-38475-9> | PubMed
59. Chen CH, Newman LN, Stark AP, Bond KE, Zhang D, Nardone S, Vanderburg CR, Nadaf NM, Yao Z, Mutume K, et al. (2023) A Purkinje cell to parabrachial nucleus pathway enables broad cerebellar influence over the forebrain. *Nat. Neurosci* **26**:1929-1941 <https://doi.org/10.1038/s41593-023-01462-w> | PubMed
60. Tong Q, Ye C, McCrimmon RJ, Dhillon H, Choi B, Kramer MD, Yu J, Yang Z, Christiansen LM, Lee CE, et al. (2007) Synaptic glutamate release by ventromedial hypothalamic neurons is part of the neurocircuitry that prevents hypoglycemia. *Cell Metab* **5**:383-393 <https://doi.org/10.1016/j.cmet.2007.04.001> | PubMed
61. Madisen L, Mao T, Koch H, Zhuo J, Berenyi A, Fujisawa S, Hsu Y.-WA, Garcia AJ, Gu X, Zanella S, et al. (2012) A toolbox of Cre-dependent optogenetic transgenic mice for light-induced activation and silencing. *Nat. Neurosci* **15**:793-802 <https://doi.org/10.1038/nn.3078> | PubMed
62. Ung K, Arenkiel BR (2012) Fiber-optic implantation for chronic optogenetic stimulation of brain tissue. *J. Vis. Exp* e50004 <https://doi.org/10.3791/50004> | PubMed
63. Yizhar O, Fenno LE, Davidson TJ, Mogri M, Deisseroth K (2011) Optogenetics in neural systems. *Neuron* **71**:9-34 <https://doi.org/10.1016/j.neuron.2011.06.004> | PubMed
64. Levy SL, White JJ, Sillitoe RV, Arenkiel BR (2015) *Neural Tracing Methods* **92** New York: Springer. pp. 51-66
65. Sillitoe RV, Stephen D, Lao Z, Joyner AL (2008) Engrailed homeobox genes determine the organization of Purkinje cell sagittal stripe gene expression in the adult cerebellum. *J. Neurosci* **28**:12150-12162 <https://doi.org/10.1523/jneurosci.2059-08.2008> | PubMed
66. Yaylaoglu MB, Titmus A, Visel A, Alvarez-Bolado G, Thaller C, Eichele G (2005) Comprehensive expression atlas of fibroblast growth factors and their receptors generated by a novel robotic in situ hybridization platform. *Dev. Dyn* **234**:371-386 <https://doi.org/10.1002/dvdy.20441> | PubMed
67. Paxinos G, Franklin KBJ (2001) *The Mouse Brain in Stereotaxic Coordinates* Elsevier Academic Press.

## Peer reviews

### Reviewer #1 (Public review):

#### Summary:

In this study, the authors aim to identify the neural circuit mechanisms underlying dystonic crisis, a severe and life-threatening manifestation of dystonia, and to explore potential therapeutic targets. The authors combine retrospective clinical data from pediatric patients with mechanistic experiments in a genetic mouse model of dystonia. They focus on inhibitory cerebellar nuclei neurons (iCNNs), testing whether these neurons can trigger dystonic crisis and whether their modulation can alleviate symptoms. Using optogenetics, anatomical tracing, and deep brain stimulation (DBS), the authors propose that iCNNs drive dystonic crisis via projections to the centrolateral (CL) thalamus and that this pathway can be therapeutically targeted.

#### Strengths:

A major strength of the study is its integrative approach, bridging human clinical observations and mechanistic animal experiments. The clinical analysis provides suggestive evidence linking cerebellar abnormalities and inhibitory signaling to dystonic crisis, which motivates the subsequent experimental work. In the mouse model, the authors use cell-type-targeted optogenetic manipulation to show that activation of iCNN pathways induces dystonic crisis-like episodes, while inhibition alleviates spontaneous crises. These bidirectional

manipulations provide strong support for a causal role of iCNN activity in modulating disease severity. The identification of a monosynaptic projection from iCNNs to the CL thalamus, combined with DBS experiments showing therapeutic effects, further strengthens the proposed circuit mechanism and highlights translational relevance.

The behavioral effects reported are robust and reproducible across animals, and the use of both activation and inhibition paradigms is a notable strength. The DBS experiments are particularly compelling in demonstrating that modulation of a downstream node can mitigate symptoms induced by upstream circuit activation, supporting the functional relevance of the identified pathway.

Weaknesses:

However, several limitations temper the strength of the conclusions.

First, the specificity of the genetic and optogenetic manipulations is not absolute. The *Ptf1a*-based strategy targets iCNNs but also labels other neuronal populations and projections, raising the possibility that off-target effects contribute to the observed phenotypes. Although the authors argue that light spread and anatomical considerations make this unlikely, more discussion on evidence of circuit specificity would strengthen the claims.

Second, the behavioral definition and quantification of "dystonic crisis" in mice, while carefully described, remain somewhat subjective and may not fully capture the complexity of the human condition. Additional quantitative or automated behavioral analyses could increase confidence in the interpretation of these episodes and facilitate comparison across conditions. If difficult to add, please at least discuss this aspect.

Third, while the anatomical tracing suggests a projection from iCNNs to the CL thalamus, the functional contribution of this specific synaptic connection is inferred rather than directly demonstrated. The DBS experiments support involvement of the CL but do not establish whether the iCNN → CL pathway is necessary or sufficient for the observed effects. More direct circuit-level manipulations would be required to fully validate this mechanism. If difficult to perform these experiments, please at least discuss the importance of such future studies.

Finally, the translational relevance, while promising, remains somewhat speculative. The clinical data are retrospective and correlative, and the therapeutic implications of targeting this pathway in humans will require further validation.

Overall, the authors have achieved their primary aim of identifying a cerebellar inhibitory circuit that can drive and modulate dystonic crisis in a mouse model. The results support their central conclusions, although some mechanistic aspects remain incompletely resolved. The study provides a valuable contribution to the field by highlighting a previously underappreciated role of inhibitory cerebellar output neurons and suggesting a new circuit-based framework for understanding and treating severe dystonia.

<https://doi.org/10.7554/eLife.111315.1.sa2>

## Reviewer #2 (Public review):

Summary:

The role of the cerebellum in producing and modifying dystonic motor phenotypes has been of increasing recent interest to understand the pathophysiology of movement disorders, as well as to develop novel pharmacological and surgical interventions to treat these disorders. Previous rodent and human imaging studies have shown that in genetic, drug-induced, and injury-acquired dystonia, cerebellar dysfunction and output from the deep cerebellar nuclei

have correlated with the development of dystonia symptoms. In some genetic dystonia patients, the strength of connections between the cerebellum, thalamus, and cortex could explain reduced penetrance or severity of symptoms in these genetically defined dystonia patients. Altogether, these studies have pointed to abnormal output from the cerebellum as a driver of abnormal motor output. Some studies have even gone as far as to suggest that no cerebellum is better than a cerebellum with abnormal output (see PMID 8491286). This indicates a critical need to understand the neural circuits underlying dystonia development, how the cerebellum drives symptom onset or severity, and if the cerebellum could be therapeutically targeted for the benefit of patients with dystonia.

Hipolito et al. use rigorous mouse genetics-based approaches to understand how a specific cell type, inhibitory projection neurons from the cerebellar nuclei, can drive dystonic phenotypes, especially severe dystonic phenotypes. The authors demonstrate a number of novel findings that further support a critical role for disturbed cerebellar output in driving dystonic phenotypes, and that disrupting this disturbed output may provide a novel therapeutic approach for dystonia. Specifically, the authors define a novel role for inhibitory neurons of the cerebellar nuclei in driving disease, and these neurons have not previously been observed to have monosynaptic connections into a specific nucleus of the thalamus. Disruption of these connections via deep-brain stimulation alleviated severe dystonic crisis with quick onset, and repeated stimulation sessions possibly had a long-term disease-modifying effect. Overall, these findings present novel insight into the circuits and mechanisms by which inhibitory neurons of the cerebellar nuclei influence dystonic states, and how these may be a viable therapeutic target for severe dystonia. My specific comments are below:

#### Strengths:

The manuscript uses rigorous mouse genetics techniques to provide fundamental insight into the role of inhibitory projection neurons of the cerebellar nuclei in influencing dystonic states. Solid experimental evidence is used to step-by-step illustrate circuit-level consequences of inhibitory projections of the cerebellar nuclei, and whether these can be manipulated for therapeutic benefit.

#### Weaknesses:

There are mild weaknesses in the approach around proving the specificity of the vGlut2 knockout, the long-term effects of silencing inhibitory projections, as well as the degree to which activation specifically drives dystonic crisis. These are addressed in my specific comments below.

<https://doi.org/10.7554/eLife.111315.1.sa1>

#### Author response:

We would like to thank the reviewers for their careful analysis of our manuscript. We appreciate their insightful suggestions for improvement. We intend to address each of their comments in our revision, with the major points outlined below.

(1) Reviewers 1 and 2 both highlighted the importance of the specificity of our genetic and optogenetic manipulations in the interpretation of our results. We agree that this point is essential. We will expand our discussion to incorporate more references demonstrating the specificity of our genetic approach, the networks engaged, and potential caveats.

(2) We acknowledge the importance of validating the dystonic nature of our model as noted by Reviewer 2 and the value of more objective quantification of dystonic crisis as requested by Reviewer 1. We will discuss the potential as well as the difficulty of developing this kind of

classification due to the non-stereotypic nature of dystonic movements and the lack of objective, measurable definitions even in clinical settings.

(3) Reviewers 1 and 2 also requested additional discussion of the role of the iCNN to CL thalamus projection in driving dystonic crisis. We will clarify our claims on this point to more accurately reflect what we can confidently interpret from our current experiments and discuss the value of further experiments in the future.

(4) We agree with Reviewers 1 and 2 that the effects of repeated stimulation are intriguing and deserve further investigation in the future. We will expand our discussion of this point to provide additional context and describe potential mechanisms that could explain our observed results, which may be tested in further studies.

(5) Reviewer 1 noted that the clinical dataset could be discussed in more detail to support the translational relevance of our findings. We will provide additional information on the characteristics of our patient sample and potential confounding variables.

<https://doi.org/10.7554/eLife.111315.1.sa0>